

Reply to Reviewer #1 comments on “Theoretical study of mixing in liquid clouds – Part 1: Classical concepts” by A. Korolev et al.

General comments to all three parts (repeated in all three reviews). I read the papers with considerable interest mostly because this seemed to be a popular topic some time ago, in both observations and modeling. I was curious to see what new these manuscripts bring. Frankly, I was disappointed. First, the analysis concerns a highly idealized problem, with little applications to real clouds. Turbulent mixing in clouds is by far more complicated than situations depicted in Fig. 1 of part 1 (and then repeated in different shapes as Figs. 1 in Part 2 and 3). Second, I am aware of a study in which the authors developed a fairly sophisticated model of microphysical evolution during turbulent stirring (Jarecka et al., JAS 2013) aiming at prediction of the homogeneity of mixing. They applied the model to LES simulations of shallow convective cloud field. The impact was surprisingly small and the authors of that paper argued why this might be so (the entrained air comes from the descending shell and is not far from saturation). So in a sense the subject is “old news”. Finally, the lengthy discussions, full of unnecessary caveats and references to details of small multi-panel figures, made the reading frustrating. All three parts read like a student dissertation, not a concise scientific paper highlighting key points and leaving the rest for the reader to follow. Thus, I read the manuscripts with decreasing interest, and my comments are more detailed for the part 1, and get more general for parts 2 and 3.

Overall, I do not believe that the subject matter deserves close to 100 pages and close to 50 figures. I feel that the material deserves a single, short and concise manuscript, with new material clearly separated from what I feel has been discussed in the past, perhaps not at such a level of detail. Reading introductions to all three parts made me mad, because all three say basically the same thing with different language and organization. Part 1 is mostly trivial in my view, with some parts speculative and other repeating already published material (see detailed comments). Parts 2 and 3 have some aspects that perhaps deserve to be published, but it is not clear to me how useful these are (not very much in my opinion). References to aircraft observations are vague and missing the key aspect, which is the irrelevance of an idealized problem considered by the authors to low-spatial resolution observations of a complicated multiscale natural system.

Reply to general comments:

Authors appreciate the Reviewer’s time and efforts to review our manuscript.

The overview sections, which were copied and pasted for all three different reviews, can be summarized by the following claims:

- a) The problem of turbulent mixing in clouds “seemed to be a popular topic some time ago”, but now “the subject is old news”.
- b) This study addresses a “highly idealized problem” and uses simplified models in order to describe cloud mixing.
- c) The results presented in the papers are not new and are “repeating already published material”.

The authors strongly disagree with the above statements of Referee 1.

In response to the first claim: the mechanism of mixing is still not well understood and continues to be a highly relevant problem in the cloud physics community, especially given the high rate of recent publications on this topic. We believe that the three papers contribute significantly to the theory of interaction of cloud droplets with turbulent environment and

present novel techniques of investigating the effect of mixing both from a theoretical standpoint and through in-situ observations.

Second, in contrast to the reviewer, we support the common practice of using idealized models of complex cloud processes, in order to investigate physical mechanisms without being bogged down by the multitude of other processes involved. Idealized considerations (e.g. adiabatic assumptions) are widely used in cloud physics as well as in physics in general. The assumptions are clearly articulated at the beginning of each paper in order to let a reader judge about the level of idealization of the utilized approaches.

Third, as regards to novelty, the following new results have been obtained:

a) The first paper suggests a new technique for identifying type of mixing (homogeneous or inhomogeneous) based of the analysis of the moments of droplet size distributions. It was shown that homogeneous mixing breaks functional relationships between the moments. Nothing like that has been done before. A novel approach for identifying mixing from in-situ observations was proposed. The comments obtained by the authors from their colleagues showed that the proposed technique start to be utilized by other research groups.

b) The second paper considers *homogeneous* mixing. One of the important finding of this paper is an analytical universal solution describing the rate of evolution microphysical parameters as well as the final equilibrium state (mixing diagram). It is shown that in case of polydisperse droplet size distributions evolution of droplet spectra can lead to increase in characteristic size of droplets in contrast to widely accepted "classical" view, when the characteristic droplet size is decreasing. It was shown that evaporation time can be expressed in terms of time of phase relaxation. This is important for definition of reaction time in Damkoller number.

c) The third paper is dedicated to *inhomogeneous* mixing. A theoretical framework for a time dependent mixing of two volumes that accompanies by cloud droplet evaporation is developed. A new turbulence-evaporation model of time evolution of ensemble of droplets under different environmental parameters is proposed. In contrast to previous studies the Damkoller number is introduced as a result of re-normalization of mixing-evaporation equation, rather than empirically. It is shown that any mixing leads to droplet spectrum broadening. For the first time the scientifically grounded demarcation between homogeneous and inhomogeneous mixing in the space of environmental parameters is performed.

The authors regret that Referee 1 overlooked all these novelties.

The authors also believe it is impossible to follow the recommendation of Referee 1, to combine all papers into one single, summary paper. While the papers all consider the same subject, they perform completely different functions with regard to investigating the issues of mixing.

Comments:

A small technical comment: I think the terminology the papers use is not correct. The limiting cases should be referred to as homogeneous and extremely inhomogeneous mixing. Everything between the two is the inhomogeneous mixing.

Reply: Corrected. The term "inhomogeneous mixing" was changed to "extreme inhomogeneous mixing" throughout the text (~47 changes, see marked-up manuscript)

Specific comments to Part 1:

1. The title should include “concepts”, not “concept”.

Reply: Corrected. The term “concept” was replaced by “concepts” in the title of the manuscript.

2. I feel the proper start to the discussion is to recognize that bulk properties (moist static energy and total water) are sufficient to calculate the final thermodynamic state (i.e., once the mixing is completed). However, the transformation of the droplet spectrum may lead to different spectra with the same final liquid water. Extremely inhomogeneous mixing leads to the final spectrum as given by (1), that is, number of droplets in each bin is simple reduced in the same proportion. Homogeneous mixing leads to a shift of the spectrum towards smaller sizes. In such a case, the shift may lead to a complete evaporation of the smallest droplets in the initial spectrum. Note that such a simple interpretation makes the first sentence in the abstract to the Part 2 trivial.

Reply: The statements about independence of the final state of the bulk parameters on the type of mixing are scattered throughout the text of Part 1. One more statement was implemented in Section 2.1 following the reviewer’s comment (lines 134-140):

“Based on mass and energy conservation considerations the final state of the bulk parameters (i.e. liquid water mixing fraction, humidity, temperature, etc.) is the same for both types of mixing. However, in the case of extreme inhomogeneous mixing saturation is reached through complete evaporation of some fraction of droplets, and their sizes remain constant. Whereas in case of homogeneous mixing saturation is reached through a uniform evaporation of droplets, and the total number of droplets remains unchanged. It should be noted, that in both cases the droplet concentration decreases due to dilution by the mixed droplet free sub-saturated parcel.”

3. The main problem with the observations is the insufficient spatial resolution. If the diluted cloud consists of filaments of cloud-free and undiluted cloudy air, averaging such a structure gives an impression of the extremely inhomogeneous mixing (this was pointed out long time ago, perhaps in on of the papers involving Charlie Knight). In fact, aircraft in-situ observations seldom allow looking at homogenized volumes, at least not at scales that the observations are able to resolve. Moreover, there are additional processes that affect droplet spectra, such as updraft and downdraft, activation of additional cloud droplets, collision/coalescence, etc.

Reply: The problem here is not as much as in the particle probe resolutions, but rather in the identification of the stage of mixing. For example, Beals et al. (2015) demonstrated existence of cloud free zones in clouds down to cm scale. That’s the highest possible spatial resolution available nowadays. However, the results of this study and other similar studies do not provide answer, whether this is a final stage of mixing and the mixing is extremely inhomogeneous, or it is an interim stage of homogeneous mixing. To address this question a collocated high spatial resolution (~1cm scale) measurements of temperature and humidity are required. Unfortunately, airborne instrument capable of such measurements are not available at that stage. The discussion about it was added in the text (lines: 604-616):

“Strictly speaking the identification of type of mixing from particle probe measurements as it was performed in Sect. 5 is incomplete. It allows establishing correlation between microphysical moments and makes a formal conclusion about the mixing type, however it does

not allow judgement about stage of mixing (i.e. whether mixing is complete by reaching equilibrium). In most previous studies, including this one, identification of type of mixing was based on the assumption that the sampled cloud volume is in equilibrium state ($RH = 1$), and that it reached the final stage of mixing (Fig.1 a2, a3, b3). It is possible that at the moment of measurement the process of mixing is not complete and the droplet free filaments remained undersaturated (Fig.1 a1, b1, b2). In this case the relationship between different moments may be well described as $M_n = \alpha_{nk}M_{nk}$ and the mixing be confused with inhomogeneous mixing.

In order to identify stage of mixing, high frequency collocated measurements of temperature and humidity are required. Unfortunately current technology does not allow such measurements yet.”

The discussion of the “non-mixing” processes (e.g. vertical velocity, WBF process etc.) affecting droplet size distribution was included in the original text. In the revised manuscript this discussion was shortened for the sake of conciseness (lines 621-635):

“Thus, collision-coalescence, riming or Wegener-Bergeron-Findeisen processes may change the droplet number concentration and liquid water content, and therefore, affect the relationship between the moments. Activation of interstitial CCN will result in breaking correlation between the moments due to formation of large concentration of droplets. Broad size distributions may also hinder identification of type of mixing due to partial evaporation of small droplets (Pinsky et al. 2015a)

It is anticipated that most suitable candidates to study mixing-entrainment process are non-precipitating convective clouds and stratocumulus clouds with relatively narrow droplet size distributions.

Another limiting factor is that the above consideration did not account for the effect of changing relative humidity in a vertically ascending parcel. Thus in droplet free entrained air RH increases approximately 10% for $\Delta z = 200\text{m}$ at $T = 0^\circ\text{C}$. After reaching saturation the mixing turns into a degenerate case, which will appear as extreme inhomogeneous mixing. Joint effects of evaporating droplets and an increase in RH during the vertical ascent may facilitate reaching saturation state. This case may also be relevant to the convective cloud described in Sect.5.2.”

4. Reference to Jarecka et al (JAS 2013) needs to be included in the paragraph starting at line 20 on p. 30213. Note that the review by Davenish et al. was published prior to that paper.

Reply: The reference to Jarecka et al. was added (line 64).

5. Section 2.2. Figure 1 shows processes occurring at a constant volume. Does it make the difference that atmospheric processes typically take place at a constant pressure?

Reply: Yes, it does. Consideration of the effect of pressure (e.g. $u_z \neq 0$) is not included in the text. This was stated in section 2.2. A potential effect of the vertical ascent was discussed in section 6. In the revised version this discussion was shortened compared to the original version (lines 630-636): “Another limiting factor is that the above consideration did not account for the effect of changing humidity in a vertically ascending parcel. Thus in droplet free entrained air relative humidity increases approximately 10% for $\Delta z = 200\text{m}$ at $T = 0^\circ\text{C}$. After reaching saturation the mixing turns into a degenerate case, which will appear as extreme inhomogeneous mixing. Joint effects of evaporating droplets and an increase in S

during the vertical ascent may facilitate reaching saturation state. This case may also be relevant to the convective cloud described in Sect.5.2.”

6. Section 2.3. Does the conservation of moist static energy and total water lead quickly to the answer?

Reply: The derivation of δq was done based on the mass and energy conservation. Yes, it leads quickly to the answer for q as long as mixing occurs in adiabatic volume. No changes were applied to the manuscript in regard to this comment.

7. I do not understand the statement below Eq. 9. Latent heating is included if one follows what I suggest in 6 above.

Reply: The mentioned statement is misleading and it was excluded from the text of the revised manuscript. The original meaning of this statement was to indicate that the temperature in Eq.9 in the original manuscript is used as a constant. The modified statement in the revised manuscript was moved to Appendix A (lines 694-697): “The process of evaporation is accompanied by changing humidity and temperature due to latent heat of vaporization. This process is described by the Eq. (C2) in Korolev and Mazin (2003). Assuming the process to be isobaric (i.e. vertical velocity $u_z = 0$) and absence of ice ($dq_i = 0$), Eq. (C2) (Korolev and Mazin, 2003) yields”

8. Section 2.4. The initial paragraph provides information that needs to be stated at the onset of the analysis (see 2 and 6 above).

Reply: The sequence of sections was rearranged in order to improve the flow of the text. The onset of the analysis is now provided in a new section 2.3 (“Effect of mixing on liquid cloud water and temperature”). The section on homogeneous mixing (original Section 2.4) is now described in Section 2.6. So, no onset is required in Sect.2.6 since it was all done in previous sections.

9. Eq. 15. The phase relaxation time scale goes back to Squires.

Reply: The reference to Squires was added (line 280).

10. Section 3. First, I do not think there is anything to model. Is the comparison between a specific model used by the authors (no details provided) and the analytical solutions the purpose of this section? Sections 3.1 to 3.4 should be compressed into a short section and a single figure should be selected. These sections are exactly what I mean by my statement that the paper reads like a student dissertation.

Reply: The main goal of section 3 is formulated as (lines 322-324): “Numerical simulations were performed to examine accuracy and limitations of the analytical expressions in Sect.2 and to conduct a sensitivity test to environmental and cloud parameters.” The authors consider that this section is important part of the manuscript to validate the equations and approach developed in sections 2.

A brief description of the model is provided at the beginning of section 3 “The simulations have been performed with the help of a parcel model similar to that in Korolev (1995). The ensemble of droplets in the simulation was assumed to be monodisperse. For the case of extreme inhomogeneous mixing the amount of evaporated water Δq required to saturate the mixed volume was calculated first. If $\Delta q < \mu q_1$, then the concentration of evaporated droplets was calculated as $N_{ev} = \frac{\Delta q}{m_d} \rho_a$, where $m_d = \pi \rho_w D^3 / 6$. Then, the concentration of the remaining droplets $N = N_1 - N_{ev}$ was recalculated based of the calculation on the volume formed after mixing. If $\Delta q \geq \mu q_1$, then all droplets evaporate, and $N = 0$. For the case of homogeneous mixing in the first step the engulfed parcel instantly mixes with the cloud parcel resulting in a new humidity RH_{m0} , temperature T_{m0} and volume V_{m0} . After that the droplets start evaporating until either their complete evaporation or saturation over liquid is reached. The calculations stopped when, either $D < 0.2\mu\text{m}$ or $(E_S - e)/E_S < 0.001$, respectively.” This description is sufficient for cloud physicist to reproduce the results in section 3.

Section 3 were shortened and rearranged (see revised manuscript with ALL marked-ups). Figs.4-6 were converted into one figure as proposed by Reviewer.

11. Section 3.5 is perhaps a good start to a follow-up investigation. At the moment, it does not belong to this paper.

Reply: This section 3.5 was turned into section 4 in the revised manuscript. This section has a direct link to the subject of the paper, which might not be well articulated in the original text. The text of section 4 underwent significant modification to make it more clear. The purpose of this section is to demonstrate a breakup of functional relationships between the microphysical moments during progressive homogeneous mixing. This has a direct link to the subject of the paper, i.e. how microphysical moments are related to each other. A physical explanation of this phenomenon is also provided in the section 4 (new Fig.10). The results of this section help interpretation of in-situ observation (conceptual diagram in Fig.12) and explain broad scattering of data points in case of homogeneous mixing. This is specifically relevant to the past studies of mixing from in-situ observations.

12. Section 3.7. This is really not a summary.

Reply: The title of this section was renamed to “Expected relationships between the moments” (line 492). The text of the former section 3.7 was rewritten and moved into Sections 5.1 in the revised manuscript.

13. Section 4 is long and does not bring anything new in my view. What is the point of having it here? I was not able to follow detailed discussion in section 4.1 and references to the specific figures. Section 4.2 can be omitted. I question the link between in-cloud observations and the results of theoretical analysis that the previous sections provide.

Reply: Section 4 (“In-situ observations”) in the original manuscript is changed to Section 5 in the revised manuscript. This section demonstrates how the results obtained in sections 2, 3 and 4 can be utilized for identification of mixing type from in-situ observations. This is a logical continuation of the theoretical study started at the beginning of the manuscript, which

ended by demonstration of its application to cloud measurements. The novel results in this section are: (1) the scattering diagrams of homogeneous and inhomogeneous mixing in Fig.12; (2) demonstration of utilizing the new approach for identification of type of mixing. Most of the previous studies to identify homogeneous mixing were based on the comparisons of measurements with the $N - r_v$ calculated for the first stage of mixing. Such attempts have a limited success and in many ways may be misleading. This section demonstrates utilization of other moments, which makes identification of type of mixing more robust.

Section 4.2 was shortened and some of its parts moved to section 6 “Discussion”. It brings up a warning that utilization of the developed approach for identification of type of mixing has limited capability and that it should not be blindly applied to a random cloud.

14. Section 5 discusses aspects that have been beaten up in other papers. Just a short paragraph with proper references would be sufficient.

Reply: The entire section on time scales was removed in the modified manuscript to make the paper more focused on the relationships between the microphysical moments.

15. Conclusion section is short, perhaps not surprisingly.

Reply: Nothing to comment.

Reply to Reviewer #2 comments on “Theoretical study of mixing in liquid clouds – Part 1: Classical concepts” by A. Korolev et al.

Overview:

The main contribution of this paper apparently is to demonstrate the relationship between different moments of the size distribution for the limits of homogeneous and extreme inhomogeneous mixing. Analytical results are compared with the results from a parcel model. The conceptual picture of inhomogeneous and homogeneous mixing is well illustrated in Figure 1 and the central analytical expression is validated in Figure 2. Figures 3-8 then show the response of different moments of the cloud droplet size distribution to idealized mixing processes. Figures 9-11 describe a conceptual model of a cascade of mixing events between a dry parcel and the cloud, which is a step toward making comparisons between the theory and observations within an evolving cloud environment. Section 4 and Figures 12-15 provide a brief analysis of observational data in the context of the conceptual models developed in the previous sections. The analysis is useful in attempting to connect the concepts and idealized models to the more complex situation observed in real clouds. The paper ends with a discussion of characteristic time scales, which seems somewhat disconnected. It is not clear how this integrates with the previous sections, and perhaps it should be either moved closer to the introduction or separated as an appendix. If kept in this location, its logical flow with the rest of the paper needs to be improved. Overall, my sense is that the expanded view to consider different moments of the size distribution is a valuable contribution, especially for the experimental cloud physics community, but perhaps also for applications to radiative transfer, remote sensing, etc. I am not aware of other papers where different moments are considered thoroughly as here, so this seems to be original. Comment regarding disconnect of the section 5 discussing the characteristic time scales.

Reply: Authors highly appreciate the Reviewer’s comprehensive comments and time to read our manuscripts. Special thanks for thoroughly going through equations and revealing numerous typos.

The manuscript underwent major revision and modification. The text was shortened to make it concise, sections were rearranged, some of them were re-written, the variable names were modified to be consistent with part 2 and 3. We agree that Section 5 is in many ways disconnected, and it was excluded from the manuscript.

General criticisms:

1. The application to size distribution moments is original, as far as I am aware (Jeffery gave a brief discussion of how the second moment is affected by mixing, but the treatment here is much more thorough and covers all typical moments). But much of the conceptual model is written more like a textbook. Maybe this is nice for readers new to the field, but the authors take a risk in expanding the length of the paper, especially when combined with the other two parts. Much more important, and definitely missing from the introduction as it currently stands, is some kind of overview of how the three part series fits together. What are the different levels of complexity treated? Why are two specialized papers on homogeneous and inhomogeneous mixing needed if part 1 already treats both cases? Now that I have read all three parts I have an idea, but this needs to be clear from the outset. It is especially important to motivate why part 1 should be connected at all. Currently it is disconnected in its approach, in its use of observational data, and even in its notation. The use of observational data is nice, but it is somewhat confusing given the title “theoretical study...” The notation is a major problem that needs to be corrected... the physics is difficult enough by itself, without having to translate symbols from one paper to the next.

Reply: The authors shortened several pages of the text in order to reduce the size of the manuscript and make it concise. A number of cross references were added in all three parts in order to link them together. As it is seen now, part 1 is closely related to part 2 and it uses the same approach. Part 3 utilizes the results of part 2. The first part uses experimental data to demonstrate the how the theoretical outcomes could be verified from in-situ measurement. In our opinion such comparisons with experimental results are natural, and if it is not there, it probably might be requested by reviewers.

We also checked Jeffery's works on mixing. However, no discussions of the effect of mixing on the DSD second moment were found. We appreciate, if this reference could be provided.

2. After a long preliminary discussion, the most important paragraph in the introduction is on page 30214 starting at Line 26: "Besides the effect on N and r the type of mixing is anticipated to manifest itself in relationships between other moments of the droplet size distribution..." It should be further explained in that paragraph why it is valuable to analyze different moments. Are they expected to be more insightful than the traditional mixing diagram methodology; is it making applications of mixing to other fields clearer; etc?

Reply: The paragraph explaining importance of the effect of mixing on the DSD moments was added in the introduction following the Reviewer's comment (lines 102-106): "It is shown that the newly obtained relationships between the moments provide a more robust identification of type of mixing from in-situ measurements as compared to conventional $N - D_v^3$ relationships used in mixing diagrams. Relationships between moments may be useful for parameterization of mixing in numerical simulations of clouds and climate, interpretations of remote sensing measurements."

3. In Fig. 9 and after, a multiple-step mixing process is envisioned. The approach is to consider mixing between a cloud and the dry environment, and then to consider subsequent mixing events between that parcel and the cloud again. Why did the authors choose to take this view instead of considering a cloud parcel progressively mixed with clear air? Some motivation for that choice is needed and some discussion of how the results would be expected to differ. For example, if one were to focus on the dry air first, dots should be concentrated at lower end in Figure 10.

Reply: The modeling of the progressive mixing presented in the paper corresponds to the case when the entrained dry air is interacting with the cloudy environment. The final state of this interaction is a diluted cloud. The progressive mixing of the cloud environment with the environmental dry air corresponds to detrainment, which ultimate state is dry cloud free air. It can be show that during detrainment the relationships between moments will be the same as during primary mixing. The authors consider that the case of detrainment is less interesting, and left it outside the frame of the manuscript in order to keep it concise. However, following the reviewers suggestion a paragraph was added in the revise manuscript in order to explain the motivation of our choice (lines 455-460): "It is worth noting that progressive mixing with the dry air does not break the functional relationships between the moments. This case is equivalent to detrainment of cloudy environment into dry air. It can be shown that Eq.(14) remain valid at any stage of progressive homogeneous mixing with dry air only, i.e.

$N_j/N_1 = \mu^{(1)} \dots \mu^{(j-1)} \mu^{(j)}$ where $\mu^{(j)}$ is the mixing fraction at the j -th stage of mixing. Eqs. (15)-(24) also remain valid for the progressive mixing with the dry air only. ”

4. There are many mistakes in the paper, including errors in the equations, at least according to the derivations as I am able to follow them. Again, the physics is difficult enough by itself, without having to make corrections. Please thoroughly check all results and the typesetting.

Reply: The authors highly appreciate the Reviewers efforts to improve our manuscript and pointing out numerous typos. All specific comments listed below were addressed and the text of the manuscript was thoroughly checked.

Specific comments

1. Eq. 1, page 30218: As monodisperse cloud droplets are used in this part of the study, the droplet size distribution $f(r)$ will confuse people. Especially Equations 2 and 3 only work for monodisperse droplets theoretically. Please explain and be consistent.

Reply: The relationships between moments are valid for relatively narrow polydisperse droplet size distributions. However, the modeling was performed for monodisperse size distributions. The confusion about assumption of monodisperse droplets during deriving relationships between the moments is probably coming from mentioning monodisperse size distributions in section 2.2. The statement about the assumption of monodispersity was removed from section 2.2 to avoid confusion.

2. Eq. 5: prefactor should be $(c_p R v T_{mo}^2 / L^2)$? T_{mo} not T_2 ?

Reply: The prefactor was corrected in the revised manuscript in Eq. (2), (former Eq.5).

3. It is difficult to connect Eq. 8 to Eq. 5. How do you prove Eq. 5 is $(1-\mu)$ Eq.8, when $T_1=T_2=T_{mo}$?

Reply: The term $(1-\mu)$ appears as a result of expansion in series. Appendix B was added to clarify the derivation of this equation.

4. Line 21, page 30218: q is liquid water mixing ratio (g/kg), not liquid water content (g/m³).

Reply: Corrected: line 251 in the revised manuscript.

5. Line 6, page 30220: The neglect of latent heat is a strong assumption that removes possible important factors such as negative buoyancy production. It is valid in the range specified by the authors, but the limitation should be discussed. Does it restrict the results to certain environments or cloud types (e.g., shallow convection)?

Reply: If fact the latent heat was accounted during derivation of Eq.3 (old Eq.8) (see Eq.A7 in Appendix A). The confusion regarding disregarding the latent heat is coming from inaccurate statement on page 30220 as indicated by Reviewer. The original purpose of this statement was to indicate that the temperature is included as a coefficient and it remains constant. In order to address the Reviewer’s concern the calculation of temperature during mixing was added in the text (line 217-219): “The temperature at the final stage of mixing can be estimated as (appendix C)

$$T = T_{m0} - \frac{(1-\mu)\delta q^* L}{c_{pa}}, \text{ when } \mu > \mu_{cr} \quad (6a)$$

$$T = T_{m0} - \frac{\mu q_1 L}{c_{pa}} \quad \text{when } \mu \leq \mu_{cr} \quad (6b)''.$$

In order to demonstrate that δq^* and δq_m allow accurate depiction of the temperature depression during mixing-evaporation process, the air temperature formed after mixing calculated from Eq. 6a,b was compared with the modelled temperature in Figs. 4h and 6h.

6. Line 7, page 30220: “comparisons of with numerical...” needs to be corrected.
Reply: Corrected: line 208 in the revised manuscript.
7. Line 13, page 30220: missing space between “on” and “delta_q”
Reply: This sentence was deleted in the revised manuscript.
8. Line 17, page 30220: the volume change due to temperature change should not affect liquid water mixing ratio, because it’s connected to mass not volume as mentioned in point 4.
Reply: This paragraph was deleted.
9. Eq. 8: prefactor should be $(c_p R v T^2 / L^2)$?
Reply: The prefactor was corrected in the revised manuscript in Eq.(4) (former Eq.8).
10. Eq. 13: left side should be r_{33}/r_{303}
Reply: Corrected: Eq.16a in the revised manuscript.
11. Eq. 14b: I think the right side should be $(q/q_0)^{2/3}(q+\delta q^*/q_0+\delta q^*)^{1/3}$
Reply: Corrected: Eq.17b in the revised manuscript.
12. Eq. 16: I believe the exponent should be $-1/3$, and inside the parentheses should be N_0/N .
Reply: Corrected: Eq.18 in the revised manuscript.
13. Eq. 20: right side should be $q^{2/3}(q+\delta q)^{1/3}/q_0$
Reply: Corrected: Eq.21 in the revised manuscript.
14. Fig. 3: it looks like panels a and b are mixed up. Also the caption refers to liquid water mixing ratio but the axis label states LWC; needs to be consistent.
Reply: Figure 3 labeling was corrected as per Reviewer comment.
15. Figs. 3 and 4: should use same format for S through the whole paper (e.g. 20% as in Fig.4 or 0.2 as in Fig. 3)
Reply: Corrected. In the revised manuscript S is replaced by RH in order to address the earlier Reviewer’s comment regarding consistency of notations with part 2 and 3. RH is determined as a saturation ratio and the RH units were adjusted throughout the text.
16. Lines 12-15, page 30224: Lots of problems here. Where are the black stars in Fig. 4? Do you mean the stars in panels (a) and (b) of Figure 3, or should there be stars in Figure 4 too? And by the

way, the stars in Figure 3 are very difficult to see... I had to search for them. And again, regarding text on line 14, the question of LWC versus q comes up. Finally, on line 15 it is not obvious to be that the statement is for Figs. 3 and 4. Do you mean to include Fig. 2 also?

Reply: Figure 4 (former Figure 3) was modified to address the Reviewer's comment. The critical mixing ratio now is indicated on all diagrams (a-h). The associated text was modified to make it consistent with the diagrams (lines 234-237): "Figure 2 shows comparisons of dependences of μ_{cr} vs. q_1 calculated from Eq. (7) and those deduced from a numerical model (Sect. 3). Critical mixing fraction μ_{cr} is also shown by black stars in Fig. 4. The locations of the stars in Fig.4 coincide well with the locations, where the modeled microphysical moments become zero."

17. Line 25, page 30226: q_0 is not liquid water content.

Reply: Corrected: line 369 in the revised manuscript.

18. Line 9 page 30227: Fig.17 should be Fig. B1?

Reply: Corrected: Figure A1 in the revised manuscript.

19. Fig. 7: why changes from $r_0=10\mu\text{m}$ (Fig. 4,5,6) to $r_0=5\mu\text{m}$. And also changes the S from 50% to 90%?

Reply: The sizes $10\mu\text{m}$ and $5\mu\text{m}$ were selected to demonstrate mixing for the cases $T_1 = T_2$ and $T_1 \neq T_2$ in a most pronounced way. For the case $RH_2=50\%$ no supersaturation will be formed. Positive supersaturation may occur only at $RH_2>80\%$ and $\Delta T<15\text{C}$. Larger ΔT seems to be uncommon for the tropospheric clouds.

20. Fig. 8: My understanding is that homogeneous and inhomogeneous mixing coincide with each other for $S_{mo}>1$? It's hard to see this phenomenon in Fig. 8 (might use different colors or symbols?) also line 5 page 30228: unclear, should be "exceed those for inhomogeneous mixing for $\Delta T=0$ and $\Delta T=5$...?"

Reply: Corrected: In the revised manuscript in Fig.7 (former Fig.8) inhomogeneous mixing for $\Delta T=10\text{C}$ is indicated by the grey circles and it coincides with the line for homogeneous mixing. For $\Delta T=0\text{C}$ homogeneous mixing line never crosses the extreme inhomogeneous line. For $\Delta T=5\text{C}$ this section is not resolved in Fig.7 due to its proximity to point (1,1). In order to clarify this issue the following text was added (lines 398-401): "However, no activation of new droplets during isobaric mixing was allowed in this study. For the cases when $RH_{m0} > 1$ (Fig. 7, AB on line 1) the condensed water was uniformly distributed between available droplets. Therefore, $q(N)$, $\beta(N)$ and $D_v(N)$ calculated for homogeneous and extremely inhomogeneous mixing coincide with each other on this interval."

21. Line 5, page 30228: in Fig. 8, ΔT is negative, here it's positive.

Reply: The associated sentence was deleted in the revised manuscript.

22. Line16, page 30228: could you explain why "the effect is more pronounced when $T_1>T_2$ compared with $T_1<T_2$."

Reply: When the entrained air is colder ($T_1>T_2$), it results in additional condensation of the cloudy air due to its cooling compared to the case when the dry air is warmer ($T_1<T_2$). This

statement is supported by the results of numerical simulations. This explanation was not included in the text for the sake of conciseness.

23. Line 27, page 30229: “becomes denser towards the top right corner” Is it because the mixed volume is mixed with cloud volume, not environmental volume?

Reply: Yes. The mixing with the cloud environment results in approaching of the properties of mixing environment to the cloud properties. Eventually the entrained air is dissolved in the cloudy environment. Again, for the sake of brevity we did not expand this explanation in the manuscript.

24. Fig. 11: why use $r_0=5$ μm , not 10 μm . It’s better to use the same radius through the paper, except you want to do the sensitivity test.

Reply: During the paper preparation the authors tried different r_0 . Unfortunately it does not work well for the same r_0 . Different r_0 (5 μm and 10 μm) were used in order to demonstrate the most pronounced effect of mixing on microstructure. A relevant comment was embedded in the text to address this issue.

25. Line 13, page 30231: missing space between “q” and “beta”

Reply: Corrected: line 498 in the revised manuscript

26. Line 14, page 30231: define Sc, Ac, Cu, Cb

Reply: This sentence was deleted in the revised version.

27. Line 1, page 30232: missing space between “N” and “q”

Reply: Corrected: line 509-510 in the revised manuscript

28. Fig. 13: caption T=-12 not -120

Reply: The caption to Fig.13 is corrected

29. Line 13, page 30233: how does sample averaging affect homogeneous versus inhomogeneous mixing?

Reply: This is a good question. It was debated over years: how the averaging scale affects identification of the type of mixing, i.e. homogeneous versus inhomogeneous? The single instrument approach used in this and the majority of previous studies does not allow judgement about type of mixing at scales smaller than the averaging scale L_{av} . In part 2 it was shown that for typical cloud environmental conditions the upper spatial scale of homogeneous mixing is limited by few m. Inhomogeneous mixing depending on the conditions may cover a wide range of scales from cm to km. A discussion of spatial scales of homogeneous and inhomogeneous mixing is provided in parts 2 and 3. Another question related to in-situ observations is whether the mixing reached equilibrium state at the moment of measurement.

30. Fig. 14a: y axis unit (g/m³) not (km⁻¹)

Reply: The y-axis label in Fig.14a was corrected following the Reviewer comment.

31. Fig. 14: what’s the dash line in a,b,d

Reply: The explanations for the dashed lined was implemented in the caption for Fig.14 (line 892): “Dashed lines are linear regressions.”

32. Line 9, page 30237: $Da \gg 1$ is for inhomogeneous mixing, while $Da \ll 1$ is for homogeneous.

Reply: This section was removed in the revised manuscript.

33. Line 14, page 30237: Andrejczuk is misspelled both here and in the reference list.

Reply: Corrected: lines 64, 749

34. Lines

35. Lines 17-22, page 30238: λ_{ev} , λ_v , and $\lambda_{\Delta V}$ need to be defined, and the assumptions in calculating them clarified (e.g., evaporating distance assumes droplet always falling at terminal speed corresponding to time-dependent radius?).

Reply: This section was removed in the revised manuscript.

36. Line 6, page 30240: S_2 approximate 1 not 0?

Reply: This section was removed in the revised manuscript.

37. Line 6, page 30240: missing space between “concentration” and “nev”

Reply: This section was removed in the revised manuscript.

38. Fig. 16: define A and B in the text or caption

Reply: This section was removed in the revised manuscript.

39. Line 13, page 30240: missing space

Reply: This section was removed in the revised manuscript.

40. Line 15, page 30240: missing space

Reply: This section was removed in the revised manuscript.

41. Eq. B4: left side should be T_{m0} not T_m

Reply: Eq. A4 (former Eq. 4B) was corrected to address the Reviewer comment.

42. Eq. B8: There seem to be mistakes here. I believe the prefactor should be $(c_p R_v T_{m0}^2 / L^2)$ and T_{m0} not T_2 ?

Reply: Eq. A8 (former Eq. B8) was rewritten so the prefactor is included in coefficient a (lines 701-704):

$$\delta q_m = -b \ln \left(\frac{1 + a RH_{m0}}{1 + a} \right) \quad (\text{A8})$$

the mixing ratio of liquid water required to evaporate in order to saturate 1 kg of the cloud volume formed after mixing with the entrained air, but before droplet start evaporating. Here

$$a = \frac{E_s R_a L^2}{p c_p R_v^2 T_{m0}^2}, \quad b = \frac{c_p R_v T_{m0}^2}{L^2}.$$

43. Line 14, page 30244: “is hold” should be “holds”?

Reply: Corrected following the reviewer comment: line 708 in the revised manuscript

44. Line 15, page 30244: Figure B1 is Figure 17.

Reply: Figure A1 numbering was corrected to address the Reviewer comment

45. Table A1: there are two τ_{ev}

46. *Reply:* The variable related to the time scale section were removed from the table.

1 **Color code for marked ups**

2 . . *Referee 1*

3 . . *Referee 2*

4 All marked up modifications can be viewed from a separately submitted file.

6 **Theoretical study of mixing in liquid clouds. Part 1: classical concepts**

8 (revised version, 14 March 2016)

10 **Alexei Korolev¹, Alex Khain², Mark Pinsky², and Jeffrey French³**

11 [1] Environment Canada, Cloud Physics and Severe Weather Section, Toronto, Canada

12 [2] Department of Atmospheric Sciences, the Hebrew University of Jerusalem, Israel

13 [3] University of Wyoming, Laramie, WY, USA

14 Correspondence to: A. Korolev (alexei.korolev@canada.ca)

16 **Abstract**

17 The present study considers final stages of in-cloud mixing in the framework of classical
18 concept of homogeneous and extreme inhomogeneous mixing. Simple analytical relationships
19 between basic microphysical parameters were obtained for homogeneous and extreme
20 inhomogeneous mixing based on the adiabatic consideration. It was demonstrated that during
21 homogeneous mixing the functional relationships between the moments of the droplets size
22 distribution hold only during primary stage of mixing. Subsequent random mixing between already
23 mixed parcels and undiluted cloud parcels breaks these relationships. However, during extreme
24 inhomogeneous mixing the functional relationships between the microphysical parameters hold
25 both for primary and subsequent mixing. The obtained relationships can be used to identify the type
26 of mixing from in situ observations. The effectiveness of the developed method was demonstrated
27 using in-situ data collected in convective clouds. It was found that for the specific set of in-situ
28 measurements the interaction between cloudy and entrained environments was dominated by
29 extreme inhomogeneous mixing.

1 Introduction

Turbulent mixing is an important non-adiabatic process in the atmosphere that to a large extent determines spatial gradients of many thermodynamic (e.g. temperature, humidity) and cloud microphysical parameters (e.g. hydrometeor concentrations, extinction coefficient, condensed water content) and as such, needs to be properly described in numerical simulations of clouds and weather predictions. Entrainment and mixing occurs during the entire lifetime of a cloud and is active not only near cloud edges, but it is important throughout the whole cloud volume. Mixing of cloudy and entrained air results in changes to the shape of the droplet size distribution through partial droplet evaporation and can also lead to changes in droplet concentration through complete evaporation of some fraction of droplets and dilution. The shape of the droplet size distribution plays key role in the initiation of precipitation and radiative properties of clouds.

The treatment of mixing in numerical simulations of clouds and precipitation formation remains a challenging problem. Besides the issues related to the way to describe mixing in numerical schemes, there is a fundamental problem of identifying a scenario or path, that mixing events should follow. Through the pioneering works of Latham and Reed (1977) and Baker et al. (1980) two explicitly alternative scenarios of mixing were identified. In the first scenario turbulent mixing rapidly stirs the environment homogenizing the fields of temperature and humidity. Following that, all of the droplets undergo partial evaporation under the same conditions. The result of this mixing is a droplet population with reduced sizes, but a total number that remains unchanged. This type of mixing is referred to as *homogeneous*. In the second scenario mixing occurs more slowly such that the population of droplets experiences different amount of sub-saturation. Some number of droplets completely evaporates, while others experience no evaporation until the entirety of the entrained air becomes saturated. Following that, turbulence mixes the rest of the droplets with the saturated, but droplet-free environment. During this type of mixing the size of droplets remains unchanged; however, their total number is reduced. This type of mixing is called *extreme inhomogeneous*. The intermediate case when some fraction of droplets evaporates partially, another other fraction evaporates completely, and a third fraction remains unchanged is in some works referred to as inhomogeneous (e.g. Baker and Latham, 1980).

The conditions for homogeneous and **extreme inhomogeneous** mixing and their effects on precipitation formation have been debated in cloud physics over forty years. There are a number of numerical simulations and theoretical efforts on studying different aspects of mixing and its effect

63 on cloud microphysics (e.g. Baker and Latham, 1982; Jensen and Baker, 1989; Su et al., 1989;
64 Lasher-Trapp et al., 2005; Jeffrey, 2007; Andrejczuk et al., 2009; Kumar et al., 2013; Jarecka et al.,
65 2013; and many others). A comprehensive review of the works on the effect of turbulence and
66 mixing on cloud droplet formation can be found in Devenish et al. (2012).

67 A number of studies were dedicated to identifying type of mixing based on in-situ observations.
68 Most of the previous observations provided evidence supporting inhomogeneous mixing (e.g. Hill
69 and Choulaton, 1985; Paluch, 1986; Bower and Choulaton, 1988; Blyth and Latham, 1991; Gerber
70 et al., 2008, Lu et al. 2011; Beals et al. 2016). However, works of Jensen and Baker (1989), Paluch
71 and Baumgardner (1989), Burnet and Brenguier (2007), Lehmann et al. (2009), Lu et al. (2011)
72 suggested occurrence of homogeneous mixing. So, at the moment it appears that both types of
73 mixing may occur in liquid clouds. However, the environmental conditions governing one or the
74 other type of mixing remain not well understood.

75 Early experimental work on identifying type of mixing from in-situ observations were based
76 on the analysis of spatial variability of the shapes of individual droplet size distributions (e.g. Paluch
77 and Knight, 1984; Paluch, 1986; Bower and Choulaton, 1988). The effectiveness of this method
78 involving the analysis of a large number of individual size spectra turned out to be quite low.
79 Another technique utilized expected functional relationships between droplet concentration (N) and
80 droplet diameter (D) specific to each type of mixing. Thus, during extreme inhomogeneous mixing
81 the droplet size is expected to remain unchanged, whereas the concentration will vary. During
82 homogeneous mixing the droplet size and concentration in cloud will be related to each other in a
83 certain way, depending on the mixing fraction and the humidity of the entrained air. This fact was
84 used in observational studies for identifying the type of mixing from “mixing diagrams” that related
85 N and D_v for different regimes of mixing (e.g. Burnet and Brenguier, 2007; Gerber et al., 2008;
86 Lehmann et al., 2009).

87 The use of mixing diagrams to some extent facilitated identification of type of mixing.
88 However, in many cases scatter in the relationships between N vs. D_v was too large, hindering
89 identification of the type of mixing (Burnet and Brenguier, 2007). To resolve this problem many
90 researchers used other complementary measurements supporting identification of the type of
91 mixing (e.g. Gerber et al., 2008; Lehmann et al., 2009).

92 Besides the effect on N and D_v , the type of mixing is anticipated to manifest itself in
93 relationships between other moments of the droplet size distribution, $f(D)$. Such relationships may

94 provide insight into the mixing process and identify type of mixing. With the exception of the work
95 by Hill and Choulaton (1985), who correlated concentration and liquid water content, there have
96 been few attempts to use any other microphysical parameters for identification of type of mixing.

97 In order to fill this gap, this study presents a theoretical analysis of relationships between
98 different moments of $f(D)$ within the framework of homogeneous and extreme inhomogeneous
99 mixing. The analysis is focused on the first four moments of $f(D)$ corresponding to the droplet
100 concentration N (0th moment), integral diameter $N\bar{D}$ (1st moment), extinction coefficient β (2nd
101 moment), liquid water mixing ratio q (3rd moment) and mean volume diameter D_v (mixed 3rd and
102 0th moment). It is shown that the newly obtained relationships between the moments provide a more
103 robust identification of type of mixing from in-situ measurements as compared to conventional $N -$
104 D_v^3 relationships used in mixing diagrams. Relationships between moments may be useful for
105 parameterization of mixing in numerical simulations of clouds and climate, interpretations of
106 remote sensing measurements.

107 This paper constitutes the first in a series of three papers. It considers the final stage of
108 mixing based on the formal definitions of homogeneous and extreme inhomogeneous mixing.
109 These two types of mixing present two extreme regimes of mixing. The following two papers
110 provide a detailed analysis of the time dependent processes during homogeneous (Pinsky et al.,
111 2016a) and inhomogeneous (Pinsky et al., 2016b) mixing where non-extreme regimes are
112 considered as well.

113 This paper is arranged in the following way. Section 2 presents analysis of the analytical
114 relationship between N , $N\bar{D}$, β , q , D_v and mixing fraction μ for the cases of homogeneous and
115 extreme inhomogeneous mixing. In Sect. 3 the obtained analytical relationships are compared with
116 the results of numerical simulation of N , β , q , D_v formed at the final stage of mixing. Section 4
117 presents results of simulation of progressive mixing and its effect on the relationships between
118 moments. Examples of relationship between N , β , q and D_v from in-situ observations are presented
119 in Sect. 5. The discussion and concluding remarks are presented in Sect. 6 and 7.

120

121 **2 Effect of mixing on microphysical variables**

122 **2.1 Phenomenological consideration**

123 The conceptual diagrams of homogeneous and extreme inhomogeneous mixing are shown on
124 Fig. 1. During the first stage of extreme inhomogeneous mixing the subsaturated parcel is engulfed

125 into the cloudy environment (Fig. 1a1). Then, the droplets at the interface of the sub-saturated parcel
126 and the cloud environment undergo complete evaporation until the air within the engulfed volume
127 reaches saturation (Fig. 1a2). After that the saturated but droplet free parcel mixes with the rest of
128 the cloud environment (Fig. 1a3). The result of inhomogeneous mixing is that the cloud parcel has
129 reduced droplet concentration and the droplet sizes remain unchanged.

130 In the case of homogeneous mixing after entraining into a cloud (Fig. 1b1), the subsaturated
131 parcel “instantly” mixes up with its cloud environment (Fig. 1b2) leading to undersaturation of the
132 total volume. Then, all droplets throughout the mixed volume undergo simultaneous evaporation
133 until the equilibrium state is reached. The result of homogeneous mixing is a cloud volume with
134 reduced concentration of droplets and droplets with reduced sizes (Fig. 1b3).

135 Based on mass and energy conservation the final state of the bulk parameters (i.e. liquid water
136 mixing fraction, humidity, temperature, etc.) is the same for both types of mixing. However, in the
137 case of extreme inhomogeneous mixing saturation is reached through complete evaporation of some
138 fraction of droplets, and their sizes remain constant. Whereas in case of homogeneous mixing
139 saturation is reached through a uniform evaporation of droplets, and the total number of droplets
140 remains unchanged. It should be noted, that in both cases the droplet concentration decreases due
141 to dilution by the mixed droplet free sub-saturated parcel.

142 The following discussion will be specifically focused on the microphysical properties formed
143 at the final stage of the homogeneous and extreme inhomogeneous mixing. The processes occurring
144 during mixing state (i.e. transition 1a→2a and 1b→2b in Fig. 1) remain outside the frame of this
145 work. Following the formalism of homogeneous and extreme inhomogeneous mixing, the process
146 of mixing reaches the final stage when (1) the entrained and cloud environment are mixed up and
147 the spatial gradients of the microphysical (N , β , q , etc.) and environmental (T , S , e , etc.) parameters
148 approach to zero; (2) the diffusional process related to droplet evaporation comes into equilibrium.
149 The second condition is completed when (a) the environment reaches saturation state, or (b) the
150 entire population of droplets is completely evaporated, if the entrained air is sufficiently dry.

151 The above description of homogeneous and extreme inhomogeneous mixing is highly
152 idealized. Actual in-cloud mixing does not occur as a sequence of discrete events (Fig.1) that
153 individually come to equilibrium only to be followed by next discrete mixing events. But rather it
154 is occurring continuously on a cascade of different spatial and time scales. Broadwell and
155 Breidenthal (1982) summarized the experimental evidence and proposed the following description

156 of mixing in turbulent shear layers. Mixing takes place in a series of events. Two shear layers
157 exchange mass by engulfing parcels from an opposite layer into localized zones. The initially large-
158 scale filaments of the two gases break down towards smaller scales due to the action of turbulence.
159 The turbulence stretches the interface between the gases and enhances the molecular diffusion
160 across the increasing surface. The actual mixing of the engulfed volume is a molecular diffusion
161 process that is most effective after the break down volumes reduce to the Kolmogorov viscosity
162 scale. It is anticipated that the reaction of the ensemble of droplets is a combination of homogeneous
163 and inhomogeneous mixing with domination of one type of mixing over the other depending on the
164 characteristic spatial and time scales of the environment determined by turbulence, cloud
165 microphysics, state parameters and stage of mixing.

166

167 **2.2 Methodology**

168 The foregoing discussion will be focused on mixing between saturated cloud parcels and out-
169 of-cloud sub-saturated air. The cloud parcel contains droplets with average diameter \bar{D}_1 , liquid
170 mixing ratio q_1 and number concentration N_1 . The initial temperature in the cloud parcel is T_1 ,
171 relative humidity $RH_1 = 1$, where $RH = e/e_s(T)$ (the explanation of variable notations is provided
172 in Table 1). The second parcel is droplet free ($N_2 = 0$), sub-saturated with initial relative humidity
173 $RH_2 < 1$ and temperature T_2 . The mixing occurs isobarically, i.e. $p = \text{const}$. At the final stage of
174 mixing the temperature and humidity formed in the resulting parcel are T and RH (appendix A).
175 The process of mixing is completed when the mixed parcel reaches equilibrium due to the air
176 saturation (i.e. $RH = 1$), or due to the complete evaporation of droplets. In the latter case the final
177 humidity is $RH \leq 1$. The effect of the vertical velocity and vertical travel on final T , RH , and q is
178 not considered here, i.e. vertical velocity $u_z = 0$.

179 Without the loss of generality the masses of the cloudy and sub-saturated volumes prior to the
180 mixing are assumed to have a unit masses, i.e. $m_1 = 1$ and $m_2 = 1$. The mixing process will be
181 considered as mixing of μ fraction of the cloud parcel with $(1 - \mu)$ fraction of the second (sub-
182 saturated) parcel. The mixing cloud fraction may vary within the range of $0 \leq \mu \leq 1$. Therefore,
183 the mass of the resulting mixed parcel is equal to $m_1\mu + (1 - \mu)m_2 = 1$. This approach simplifies
184 the consideration of mixing and allows considering all possible proportions of the mixing of two
185 volumes.

186

2.3 Effect of mixing on liquid water and temperature

The mixing ratio of liquid water q formed at the final stage of mixing is determined by the mass of the mixing cloud water μq_1 and amount of evaporated water required to saturate the newly formed mixed volume δq_m . The mass balance of liquid water for the mixing volume yields

$$q = \mu q_1 - \delta q_m, \quad (1)$$

where

$$\delta q_m = \frac{c_p R_v T_{m0}^2}{L^2} \ln \left(\frac{1 + \frac{e_s(T_{m0}) R_a L^2}{p c_{pa} R_v^2 T_{m0}^2}}{1 + RH_{m0} \frac{e_s(T_{m0}) R_a L^2}{p c_{pa} R_v^2 T_{m0}^2}} \right) \cong -\frac{S_{m0}}{A_2} \quad (2)$$

is the mixing ratio of liquid water required to saturate 1kg of volume with temperature T_{m0} and humidity RH_{m0} (appendix A); T_{m0} , RH_{m0} and S_{m0} , are the temperature, relative humidity formed and supersaturation formed in the volume after instantaneous air mixing, but before droplets start evaporating (appendix A); $e_s(T_{m0})$ is saturation vapor pressure at temperature T_{m0} .

Eq. (1) is a non-linear function of μ , since T_{m0} , e_{m0} and thus δq_m depend on μ . Eq.(1) can be simplified, if $T_1 = T_2$. In this case $T_{m0} = T_1 = T_2$, and $e_s(T_{m0}) = e_s(T_1) = e_s(T_2)$. Given that, the expression under logarithm in Eq.(2) can be expanded in series resulting in (appendix B)

$$\delta q_m = (1 - \mu) \delta q^*, \quad (3)$$

where

$$\delta q^* = \frac{c_p R_v T_2^2}{L^2} \ln \left(\frac{1 + \frac{e_s(T_2) R_a L^2}{p c_{pa} R_v^2 T_2^2}}{1 + RH_2 \frac{e_s(T_2) R_a L^2}{p c_{pa} R_v^2 T_2^2}} \right) \cong -\frac{S_2}{A_2} \quad (4)$$

is the mixing ratio of liquid water required to saturate 1 kg of the entrained dry air. Substituting Eq.(3) in Eq.(1) gives

$$q = \mu q_1 - (1 - \mu) \delta q^*, \quad (5)$$

The value of δq^* does not depend on μ , and Eq. (5) is a simple linear function of μ . The comparisons with numerical simulations showed, that Eq.(5) provides accuracy within few percent, when the temperature difference $|T_1 - T_2| < 2^\circ\text{C}$. Although, in many cases $|T_1 - T_2|$ may vary a wide range reaching 10°C or higher, clouds with $|T_1 - T_2| < 2^\circ\text{C}$ are quite common. Therefore, for

211 the sake of simplicity, Eq.(5) and the assumption $T_1 \approx T_2$ will be used in the following consideration
 212 of mixing.

213 It should be noted that, Eqs (1) and (5) are valid for the cases, when $\mu > \mu_{cr}$. Here μ_{cr} is critical
 214 mixing fraction, which separates partial and complete evaporation of cloud water in the mixing
 215 volume (section 2.4). Cases when $\mu \leq \mu_{cr}$ correspond to complete evaporation of droplets, and $q =$
 216 0.

217 The temperature at the final stage of mixing can be estimated as (appendix C)

$$218 \quad T = T_{m0} - \frac{(1-\mu)\delta q^* L}{c_{pa}}, \quad \text{when } \mu > \mu_{cr} \quad (6a)$$

$$219 \quad T = T_{m0} - \frac{\mu q_1 L}{c_{pa}} \quad \text{when } \mu \leq \mu_{cr} \quad (6b)$$

220 Eqs. (1), (5), (6) were obtained based on mass and energy conservation, and they do not depend
 221 on how mixing proceeds. Therefore, Eqs. (1), (5), (6) are valid for both homogeneous and
 222 inhomogeneous mixing.

223

224 2.4 Complete evaporation

225 As mentioned in section 2.2 the process of mixing is complete only after reaching equilibrium
 226 by saturating the mixed volume or by evaporating of all cloud droplets depending on the mixing
 227 fraction μ . The critical mixing fraction μ_{cr} , corresponding to evaporation of all droplets, can be
 228 found from Eq.(5) when $q = 0$, i.e.

$$229 \quad \mu_{cr} = \frac{\delta q^*}{q_1 + \delta q^*} \quad (7)$$

230 Critical mixing fraction separates μ in two subranges: (a) $1 \geq \mu > \mu_{cr}$ where q is described by
 231 Eqs.(1) or (5) and $RH_m = 1$; (b) $\mu_{cr} \geq \mu \geq 0$ where $q = 0$ and $RH_m \leq 1$.

232 For the general case when $T_1 \neq T_2$, μ_{cr} , can be found by solving the non-linear equation

$$233 \quad \mu_{cr} q_1 - \delta q_m(\mu_{cr}) = 0 \quad (8)$$

234 Figure 2 shows comparisons of dependences of μ_{cr} vs. q_1 calculated from Eq. (7) and those
 235 deduced from a numerical model (Sect. 3). Critical mixing fraction μ_{cr} is also shown by black stars
 236 in Fig. 4. The locations of the stars in Fig.4 coincide well with the locations, where the modeled

237 microphysical moments become zero. The obtained agreement between analytical and modeled μ_{cr}
 238 in Figs. 2 and 4 validates the developed approach.

239

240 **2.5 Extreme inhomogeneous mixing**

241 Within the framework of extreme inhomogeneous mixing some fraction of droplets undergo
 242 complete evaporation, whereas the rest of the droplets remain unchanged. Therefore, such a process
 243 results in scaling the droplet size distribution $f(D)$, i.e.

$$244 \quad f(D) = kf_1(D) \quad (9)$$

245 where k is some coefficient dependent on μ and the initial environmental parameters of the mixing
 246 volumes, $f_1(D)$ is the droplet size distribution before mixing. Equation (9) yields relationships
 247 between pairs n th and k -th moments

$$248 \quad \frac{M_n}{M_{n1}} = \frac{M_k}{M_{k1}} \quad (10)$$

249 where $M_n = \int_0^\infty f(D)D^n dD / \int_0^\infty f(D)dD$ is the n th moment of $f(D)$. Therefore, it is anticipated that

250 for extreme inhomogeneous mixing droplet number concentration N (0th moment), extinction
 251 coefficient β (2nd moment), liquid water mixing ratio q (3rd moment), along with other moments,
 252 will correlate with each other, i.e.

$$253 \quad \frac{N}{N_1} = \frac{\beta}{\beta_1} = \frac{q}{q_1} \quad (11)$$

254 One of the consequences of Eqs. (9)-(11) is that the characteristic droplet sizes \bar{D} , D_2 , D_v , D_{eff}
 255 will remain constant during inhomogeneous mixing.

256 For the case $T_1 = T_2$ and $\mu > \mu_{cr}$ Eqs. (5) and (11) yield the dependence of N vs. μ

$$257 \quad N = N_1 \left(\mu - \frac{(1-\mu)\delta q^*}{q_1} \right) \quad (12)$$

$$258 \quad \beta = \beta_1 \left(\mu - \frac{(1-\mu)\delta q^*}{q_1} \right) \quad (13)$$

259 For a general case when $T_1 \neq T_2$ the term $(1-\mu)\delta q^*$ in Eqs. (12) and (13) should be replaced
 260 by $\delta q_m(\mu)$ (Eq.(2)).

261

2.6 Homogeneous mixing

For homogeneous mixing, when $\mu > \mu_{cr}$, the droplet number concentration changes only due to dilution by the entrained air, i.e.

$$\frac{N}{N_1} = \mu \quad (14)$$

Assuming $T_1 = T_2$, and substituting Eq. (5) in (14) yields:

$$\frac{N}{N_1} = \frac{q + \delta q^*}{q_1 + \delta q^*} \quad (15)$$

As follows from Eq. (15) N and q are linearly related for homogeneous mixing. However, no linear relationships exist between other moments. Thus, substituting the definition of the liquid water mixing ratio $q = \pi \rho_w N D_v^3 / 6 \rho_a$ in Eq. (15) yields the relationship between mean volume droplet size and concentration

$$\frac{D_v^3}{D_{v1}^3} = 1 + \left(1 - \frac{N_0}{N}\right) \frac{\delta q^*}{q_1} \quad (16a)$$

$$\frac{D_v^3}{D_{v1}^3} = \frac{q}{q_1} \left(\frac{q_1 + \delta q^*}{q + \delta q^*} \right) \quad (16b)$$

In a similar way the relationship between the extinction coefficient $\beta = Q \pi N D_2^2 / 4$, N and q can be written as

$$\frac{\beta}{\beta_1} = \frac{N}{N_1} \left(1 + \left(1 - \frac{N_0}{N}\right) \frac{\delta q^*}{q_1} \right)^{2/3} \quad (17a)$$

$$\frac{\beta}{\beta_1} = \left(\frac{q}{q_1} \right)^{2/3} \left(\frac{q + \delta q^*}{q_1 + \delta q^*} \right)^{1/3} \quad (17b)$$

In Eqs. (17a) and (17b) it is assumed that $D_2 \approx D_v$.

Substituting in Eq. (16) the expression for the time of phase relaxation $\tau_p = 1/bN\bar{D}$ (e.g. Squires 1953; Korolev and Mazin, 2003) and assuming $\bar{D} \approx D_v$ yields

$$\frac{\tau}{\tau_1} = \frac{N_1}{N} \left(1 + \left(1 - \frac{N_1}{N}\right) \frac{\delta q^*}{q_1} \right)^{-1/3} \quad (18)$$

For the cases when the temperature difference $|T_1 - T_2|$ exceeds a few degrees, the effect of μ on T_m and S_m should be taken into consideration in the calculations of evaporated water. For such

284 cases δq_m (Eq. (2)) should be used instead of δq^* . Using Eq. (14) δq_m can be presented as a
 285 function of $\frac{N}{N_1}$, i.e. $\delta q_m(\mu) = \delta q_m\left(\frac{N}{N_1}\right)$. Replacing Eq. (5) by (1) in the above consideration, the
 286 equations Eqs. (15)-(18) can be rewritten as

$$287 \quad \frac{N}{N_1} = \frac{q + \delta q_m\left(\frac{N}{N_1}\right)}{q_1} \quad (19)$$

$$288 \quad \frac{D_v^3}{D_{v1}^3} = 1 - \frac{\delta q_m\left(\frac{N}{N_1}\right) \frac{N_1}{N}}{q_1} = \frac{q}{q + \delta q_m\left(\frac{q}{q_1}\right)} \quad (20)$$

$$289 \quad \frac{\beta}{\beta_1} = \frac{N}{N_1} \left(1 - \frac{\delta q_m\left(\frac{N}{N_1}\right) \frac{N}{N_1}}{q_1} \right)^{2/3} = \frac{q^{2/3} \left(q + \delta q_m\left(\frac{\beta}{\beta_1}\right) \right)^{1/3}}{q_1} \quad (21)$$

$$290 \quad \frac{\tau_p}{\tau_{p1}} = \frac{N_1}{N} \left(1 - \frac{\delta q_m\left(\frac{N}{N_0}\right) \frac{N_1}{N}}{q_1} \right)^{-1/3} \quad (22)$$

291 Eqs. (19)–(22) can be solved numerically.

292

293 **2.7 Degenerate case**

294 As follows from Eq.(5), if

$$295 \quad \frac{(1-\mu) \delta q^*}{\mu q_1} \ll 1 \quad (23)$$

296 then $q_1 \geq q \gg \delta q^*$. If the condition in Eq. (23) is valid, then the terms associated with δq^* in Eqs.
 297 (15)-(18) can be neglected. This results in correlation of all moments, i.e. $N/N_1 = \beta/\beta_1 = q/q_1$
 298 (compare with Eq.(11)). This corresponds to the degenerate case, when the difference between the
 299 homogeneous and inhomogeneous mixing vanishes. Thus, the dimensionless parameter $\xi =$
 300 $\frac{1-\mu}{\mu} \frac{\delta q^*}{q_1}$ can be used for characterization of proximity of the homogeneous mixing moments to those
 301 formed during extremely inhomogeneous mixing.

302 The range of μ in ξ is limited by $\mu_{cr} < \mu \leq 1$, so that $0 < \frac{1-\mu}{\mu} \leq \frac{q_1}{\delta q^*}$. This gives the range of
 303 changes of ξ , i.e. $0 \leq \xi \leq 1$ for the mixing without complete evaporation of droplets. The
 304 degenerate case corresponds to $\xi \rightarrow 0$, whereas $\xi \rightarrow 1$ corresponds to maximum difference of the
 305 moments for homogeneous and extremely inhomogeneous mixing.

306 As follows from Eqs. (4) and (23) approaching to the degenerate case ($\xi \rightarrow 0$) occurs, when
 307 one of the following conditions or their combination is satisfied: (a) $RH_2 \rightarrow 1$; (b) $E_s(T) \rightarrow 0$ at
 308 low temperatures; (c) $q_1 \gg \delta q^*$; (d) $\mu \rightarrow 1$. The effect of RH , T , q_1 and μ on mixing will be
 309 demonstrated in Sect.3.

310 Figure 3 shows dependence of ξ vs. μ . The grey area in Fig.3 indicates the region where
 311 identification of type of mixing from in-situ measurements (Sect.5) may be hindered due to
 312 proximity of the moments for homogeneous and inhomogeneous mixing. Thus for $\delta q^*/q_1 = 0.01$
 313 identification of type of mixing is ambiguous for nearly the entire range of μ .

314 For the general case, when $T_1 \neq T_2$, it should be $\xi = \frac{|\delta q_m(\mu)|}{\mu q_1}$. An absolute value $|\delta q_m(\mu)|$
 315 should be used in ξ since $\delta q_m(\mu)$ can be negative (Appendix A, Fig.A1) if mixing results in
 316 supersaturation Sect. 3.4).

317 The coefficient ξ may be useful for identification type of mixing from in-situ observations. It
 318 is worth nothing, that the ratio $\frac{\delta q^*}{q_1} \cong \frac{S_2}{A_2 q_1}$ is equal to the parameter R (Pinsky et al. 2015ab), which
 319 plays an important role in determining scenarios of droplet evaporation in turbulent environment.

320

321 **3 Comparisons with numerical simulations**

322 Numerical simulations were performed to examine accuracy and limitations of the analytical
 323 expressions in Sect.2 and to conduct a sensitivity test to environmental and cloud parameters. The
 324 simulations have been performed with the help of a parcel model similar to that in Korolev (1995).
 325 The ensemble of droplets in the simulation was assumed to be monodisperse. For the case of
 326 extreme inhomogeneous mixing the amount of evaporated water Δq required to saturate the mixed
 327 volume was calculated first. If $\Delta q < \mu q_1$, then the concentration of evaporated droplets was
 328 calculated as $N_{ev} = \frac{\Delta q}{m_d} \rho_a$, where $m_d = \pi \rho_w D^3 / 6$. Then, the concentration of the remaining
 329 droplets $N = N_1 - N_{ev}$ was recalculated based of the calculation on the volume formed after
 330 mixing. If $\Delta q \geq \mu q_1$, then all droplets evaporate, and $N = 0$.

331 For the case of homogeneous mixing in the first step the engulfed parcel instantly mixes with
332 the cloud parcel resulting in a new humidity RH_{m0} , temperature T_{m0} and volume V_{m0} . After that
333 the droplets start evaporating until either their complete evaporation or saturation over liquid is
334 reached. The calculations stopped when, either $D < 0.2\mu\text{m}$ or $(E_S - e)/E_S < 0.001$, respectively.

335

336 3.1 Effect of mixing fraction

337 Figure 4 shows the results of the simulation of different moments and state parameters vs. μ .
338 The calculations were performed for different relative humidity of the entrained parcel $RH_2 = 0.2,$
339 $0.5, 0.8$ and 0.95 . As seen from Fig.4 for the case of homogeneous mixing only N and q are linearly
340 related with μ , the rest of the variables have non-linear dependences on μ . For the case of
341 inhomogeneous mixing all $f(D)$ moments and droplet sizes linearly depend on μ . Note, for $\mu \leq$
342 μ_{cr} all moments are equal to zero.

343 Since the amount of the evaporated liquid water does not depend on the type of mixing, the
344 dependences of $q(\mu)$ are the same for both homogeneous and inhomogeneous mixing (Fig.4a). The
345 type of mixing has the most pronounced effect on the droplet concentration (Fig.4b) and droplet
346 sizes (Fig.4e).

347 Figure 4g shows the dependences RH_{m0} and RH vs. μ , Here RH_{m0} is the relative humidity at
348 the initial stage of homogeneous mixing before droplets start evaporating (Fig. 1b2). Figure 3h
349 presents comparisons of modeled $T(\mu)$ and those calculated from Eqs.(6a,b) and (C4). The
350 independence of $q(\mu)$, $RH(\mu)$ and $T(\mu)$ on type of mixing (Fig.4a,g,h) is the consequence of the
351 mass and energy conservation, which are not contingent on type of mixing.

352

353 3.2 Effect of humidity of entrained air

354 The diagrams in Fig. 5a-c show the dependences of normalized β , q and D_v vs. N/N_0
355 calculated from numerical simulations and analytical equations from Sect. 2. The calculations were
356 performed for different humidity of the entrained air RH_2 . As seen from Fig. 5a-c, the normalized
357 dependences for homogeneous mixing $q(N)$, $\beta(N)$ and $D_v(N)$ tend to approach the line of **extreme**
358 **inhomogeneous** mixing when relative humidity RH_2 approaches to 1. This is consistent with the
359 degenerate case, when $\xi \rightarrow 0$ (Sect.2.7). In this case droplets behave as a passive admixture, and
360 they do not interact with the environment.

361

3.3 Effect of liquid water mixing ratio

Figure 5d-f demonstrate the sensitivity of $q(N)$, $\beta(N)$ and $D_v(N)$ to liquid water mixing ratio q_1 . It is seen, that the increase of q_1 results in $q(N)$, $\beta(N)$ and $D_v(N)$ (calculated for homogeneous mixing) approaching towards $q(N)$, $\beta(N)$ and $D_v(N)$ for the inhomogeneous mixing. In other words, the sensitivity of the microphysical parameters to the type of mixing increases with the decrease of q_1 . From a practical viewpoint it means, that from in-situ observations the difference between homogeneous and inhomogeneous mixing is anticipated to be more pronounced for the cases with a relatively low liquid water mixing ratio (e.g. $q_1 < 1 \text{ g/kg}$). Such behaviour is consistent with the consideration in Sect. 2.7.

3.4 Effect of temperature $T_1 = T_2$

Figure 5g-j shows the effect of temperature on the normalized $q(N)$, $\beta(N)$ and $D_v(N)$ for $T_1 = T_2$. Figure 5g-j indicate that the difference between the moments becomes most pronounced at warm temperatures, whereas at cold temperatures (e.g. $T = -30^\circ\text{C}$), $q(N)$, $\beta(N)$ and $D_v(N)$ for homogeneous mixing are approaching those for the extreme inhomogeneous mixing limit.

Such behavior is explained by the fact that liquid water deficit δq_m decreases with decreasing temperature (appendix A, Fig. A1). At low temperatures ($T = -30^\circ\text{C}$) the amount of evaporated water δq_m is so small, that homogeneous mixing with dry out-of-cloud air will have approximately the same effect as mixing with saturated air (i.e. degenerate case, Sect. 2.7).

Overall, as follows from Fig.5 the results the analytical predictions (Sect. 2) turned out to be in a good agreement with numerical simulations.

3.5 Effect of temperature $T_1 \neq T_2$

Isobaric mixing of two nearly saturated volumes with $T_1 \neq T_2$ may result in supersaturated environment (e.g. Rogers, 1976; Bohren and Albrecht, 1998). Mixing resulting in supersaturation is different in principle from the mixing with evaporating droplets. In this case the meaning of homogeneous and inhomogeneous mixing becomes ambiguous. Formation of supersaturation leads to different dependences between $N\bar{D}$, β , q , \bar{D} and N as compared to those shown in Figs. 3–4, when $T_1 = T_2$.

Figure 6 presents a set of diagrams similar to those in Fig.4, but calculated for the cases when $T_1 \leq T_2$. It turns out that for the case of extreme inhomogeneous mixing the temperature difference

393 between T_1 and T_2 breaks down linear dependences of the microphysical moments (e.g. $N\bar{D}$, β , q
394 Fig. 6a,c,d) vs. μ .

395 Figure 7 presents the effect of the temperature difference ΔT on the normalized dependences
396 $q(N)$, $\beta(N)$ and $D_v(N)$. In clouds, high supersaturation resulting from isobaric mixing may lead to
397 activation of interstitial CCN, which may increase N and decrease D_v (Korolev and Isaac, 2000).
398 However, no activation of new droplets during isobaric mixing was allowed in this study. For the
399 cases when $RH_{m0} > 1$ (Fig. 7, AB on line 1) the condensed water was uniformly distributed
400 between available droplets. Therefore, $q(N)$, $\beta(N)$ and $D_v(N)$ calculated for homogeneous and
401 extremely inhomogeneous mixing coincide with each other on this interval.

402 Numerical simulations also showed, that the effect of temperature on mixing is more
403 pronounced for the cases when the cloud temperature is warmer than that of the entrained air, i.e.
404 $T_1 > T_2$, as compared to the cases with $T_1 < T_2$.

405

406 **4. Progressive mixing**

407 **4.1 Effect on microphysical parameters**

408 In the previous sections the mixing was considered as a single event, i.e. μ fraction of the cloudy
409 air mixed up with $(1 - \mu)$ fraction of entrained dry air. Such mixing will be referred to as “primary”
410 mixing. Primary mixing results in an ensemble of elementary volumes characterized by a set of
411 microphysical and state parameters i.e. $\bar{D}(\mu)$, $N(\mu)$, $RH(\mu)$, $T(\mu)$, etc. Each of these parameters
412 has a functional dependence on μ , and what is important, these parameters have functional
413 relationships between each other.

414 In reality mixing is a continuous process. It does not stop after the primary mixing. The
415 elementary volumes formed after primary mixing continue to progressively mix with each other.

416 The second stage of mixing will result in an ensemble of elementary volumes characterized by
417 a set of parameters $D_v^{(2)}$, $N^{(2)}$, $RH^{(2)}$, $T^{(2)}$, etc. Here the superscript ⁽²⁾ indicates the stage of mixing.
418 After the second stage the mixed volumes undergo subsequent stages of mixing.

419 The idealised conceptual diagram of the progressive mixing is shown in Fig. 8. As mentioned
420 in Sect. 2.1, the actual process of mixing is indeed much more complex than the sequence of discrete
421 events portrayed in Fig.8. However, as it will be shown below, this simplified consideration of
422 allows establishing main features of evolution of relationships between the microphysical moments

423 affected by mixing. The obtained results facilitates identification of type of mixing from in-situ
424 measurements.

425 Progressive mixing was simulated with the help of a numerical model, where parcels were
426 randomly mixed with each other and with the cloud environment. The mixing fraction μ was also
427 set to be random during each mixing event. Models of stochastic mixing have been used in a number
428 of studies (e.g. Krueger et al., 1997; Su et al., 1998; Burnet and Brenguier, 2007). In the present
429 work the analysis of progressive mixing is expanded to examine its effect on the relationship
430 between moments of the droplet size distribution.

431 The results of the progressive mixing for the first four stages are presented in Fig. 9. As seen
432 from Fig. 9 the functional relationship between the pairs of microphysical and state parameters
433 exists only for the primary stage. For higher mixing stages these functional relationships break
434 down. Thus, cloud volumes with the same $N^{(2)}$ may have different $D_v^{(2)}$. Figure 9 also shows that
435 the regions of scattering of $q(N)$, $\beta(N)$ and $D_v(N)$ for stages 2, 3 and 4 are limited from above by
436 the inhomogeneous mixing (red dashed lines) and from below by primary homogeneous mixing
437 (red solid lines).

438 Figure 10 presents a conceptual $N - q$ diagram explaining breaking the functional relationships
439 during progressive homogeneous mixing. After the first stage of mixing the $N - q$ points will be
440 scattered along the line OB and point C . The line OB corresponds to the ensemble of points with
441 $RH = 1$. Therefore, result of mixing between two saturated volumes randomly selected on AB , will
442 remain on the same line. Point C corresponds to the ensemble of points with $N = 0$, $RH_2 \leq$
443 $RH_C(\mu^{(1)}) \leq 1$, where $0 \leq \mu^{(1)} < \mu_{cr}$. Therefore, mixing between point A (Fig.10) and point C ,
444 when $RH = 1$ will result in scattering along the line AC (degenerate case). Points resulted from
445 mixing between A ($RH = 1$) and point C , when $RH_2 \leq RH_C < 1$, will scattered over the ensemble
446 of dashed lines shown in Fig.10. These lines will fill the sector CAB . Random mixing between
447 points on the line OB and C , will eventually fill the entire sector COB . The same consideration can
448 be applied to progressive mixing between other moments.

449 During the progressive mixing $N^{(n)}$, $\beta^{(n)}$, $q^{(n)}$ and $D_v^{(n)}$ formed in the elementary parcels tend
450 to approach those in the undiluted cloud, i.e. N_1 , β_1 , q_1 and D_{v1} . This process can be considered as
451 a surrogate to the diffusion process between the cloud and sub-saturated out-of-cloud environment.
452 The convergence of $\beta^{(n)}$, $q^{(n)}$ and $D_v^{(n)}$ during the progressive mixing can be seen in Fig. 9, where

453 the scattering of normalized $q^{(n)}(N)$, $\beta^{(n)}(N)$ and $D_v^{(n)}(N)$ becomes denser towards the top-right
454 corner (1,1) with the increase of the stage of mixing.

455 It is worth noting that progressive mixing with the dry air does not break the functional
456 relationships between the moments. This case is equivalent to detrainment of cloudy environment
457 into dry air. It can be shown that Eq.(14) remain valid at any stage of progressive homogeneous
458 mixing with dry air only, i.e. $N_j/N_1 = \mu^{(1)} \dots \mu^{(j-1)} \mu^{(j)}$, where $\mu^{(j)}$ is the mixing fraction at the
459 j -th stage of mixing. Eqs. (15)-(24) also remain valid for the progressive mixing with the dry air
460 only.

461 As follows from Eq. (9) for the case of extreme inhomogeneous mixing the progressive mixing
462 does not affect the functional relations between $N^{(n)}$, $\beta^{(n)}$, $q^{(n)}$ and $D_v^{(n)}$ and other microphysical
463 parameters. These relations remain the same regardless of the actual stage of mixing. This is one of
464 the fundamental differences between homogeneous and inhomogeneous mixing, which can be used
465 for identification of type of mixing from in-situ measurements.

466

467 **4.2 Effect on droplet size distributions**

468 Figure 11 shows modeled droplet size distributions averaged over the ensembles of elementary
469 volumes corresponding to the first four stages of homogeneous mixing. As seen from Fig. 11a–d
470 for the case with $T_1 = T_2$ the droplet size distributions are broadened towards small sizes.
471 Depending on the stage of mixing and mixing fraction μ the size distributions formed in each
472 elementary volume may be unimodal or multimodal. However, due to the random nature of the
473 modal sizes formed during mixing, the average size distributions become smooth and unimodal
474 (Fig.11a-d).

475 Broadening of droplet size distributions towards small sizes during homogeneous mixing is
476 well known and it was demonstrated in a number of studies (e.g. Baker and Latham, 1982; Jensen
477 and Baker, 1989; Jeffery, 2007; Kumar et al., 2013). However, if mixing results in supersaturation
478 (section 3.4), then the droplet size distribution may broaden towards larger sizes (Fig. 11e–h). For
479 this to occur, both the temperature difference between the cloud and the environment $|T_1 - T_2|$ and
480 the relative humidity of the environment RH_2 must be sufficiently large. Such conditions are
481 inherently unstable, however, this might occur in regions that have been moistened through prior
482 cloud detrainment. Thus homogeneous mixing may result in broadening of droplet size distributions
483 towards either smaller or larger sizes (Fig.11).

484 These results were obtained in the frame of the formalism of homogeneous and inhomogeneous
485 mixing. The following two works in this series (Pinsky et al., 2016a, b) will discuss the broadening
486 of polydisperse and monodisperse $f(D)$ during both homogeneous and inhomogeneous mixing in
487 greater details.

488

489 **5 Identification of type of mixing from in-situ observations**

490 The purpose of this section is to attempt identifying type of mixing based on examining
491 relationships between basic microphysical parameters N , β , LWC , D_v measured from in-situ.

492 **5.1 Expected relationships between the moments**

493 Prior proceeding with the analysis of in-situ data we summarize the results of the previous
494 consideration on how homogeneous and **extreme inhomogeneous** mixing is expected to manifest
495 itself in relationships between basic microphysical parameters, such as N , β , q and D_v .

496 For **extreme inhomogeneous** mixing the relationship between the pairs of N , β and q are
497 determined by linear dependences $M_n = \alpha_{nk}M_k$ (Eq. 10) at any stage of mixing. As follows from
498 Eq. (11) the slopes α_{nk} for $q(N)$, $\beta(N)$ and $q(\beta)$ are equal to the ratios q_1/N_1 , β_1/N_1 , and q_1/β_1 ,
499 respectively, where N_1 , β_1 and q_1 correspond to undiluted adiabatic values. The values of N_1 , β_1
500 and q_1 may vary depending on the location inside the cloud and environmental conditions at the
501 cloud base. Thus, the adiabatic value of q_1 is a function of elevation above the cloud base ΔZ ,
502 whereas N_1 depends on the vertical velocity at the cloud base u_z and the aerosol load. Therefore,
503 the scattering of $q - N$ points will be aligned along an ensemble of different lines determined by
504 q_1/N_1 , which are specific to different cloud volumes. The conceptual diagram of the scattering of
505 $q - N$ measurements in a cloud with **extreme inhomogeneous** mixing is shown in Fig. 12a. The
506 scatter diagrams for other moments (e.g. $q - \beta$, $N - \beta$) will have the similar patterns as that in Fig.
507 12a.

508 For the case of homogeneous mixing the functional relationship between the pairs of N , β , q
509 and D_v are disrupted by a progressive mixing. As shown in Sect. 4.1 the ensemble of points of N ,
510 β and q will be scattered within a sector, which is limited by lines determined by Eq. (11) (**extreme**
511 **inhomogeneous** mixing) and Eqs. (15)-(17) (primary homogeneous), respectively (Fig. 9). What is
512 important, is that the top of the sectors for $q(N)$ and $\beta(N)$ correspond to points $[N_1, q_1]$ and $[N_1, \beta_1]$,
513 respectively. Since N_1 , β_1 and q_1 may vary within the same cloud, it is anticipated that the N , β and
514 q measurements will be scattered within an ensemble of sectors as shown in Fig. 12b.

515 It is important to note that that during homogeneous mixing prior reaching equilibrium,
516 functional relationships between the microphysical moments do not exist either. After the instant
517 mixing of cloud fraction μ with entrained air (Fig. 1b(2)), $q_{m0} = \mu q_0$ and $N_{m0} = \mu N_0$. This state
518 corresponds to point D in Fig.10. After that droplets start evaporating until liquid mixing ratio
519 reaches point A (Fig.10), which corresponds to the equilibrium state ($RH = 1$). Therefore, during
520 evaporation time $q - N$ points will be scattered along the line AD . Since, point D can be located
521 anywhere on OC , the ensemble of $q - N$ points corresponding to non-equilibrium state will fill the
522 COB area.

523 Thus, the absence of the functional relationships between the moments during homogeneous
524 mixing may occur both during progressive mixing and during primary mixing prior reaching the
525 equilibrium state. The evaporation time required to reach equilibrium during homogeneous mixing
526 is discussed in details in Pinsky et al. (2016b), and it is usually limited by few tens of seconds.
527 However, progressive mixing is not limited in time. Therefore, it is very likely that no functional
528 relationship between microphysical parameters will be observed during in-situ measurements.

529 Fig.12 demonstrated a fundamental difference in scattering of $q - N$ for homogeneous and
530 **extreme inhomogeneous** mixing, which will be used to facilitate identification of type of mixing in
531 the following section.

532

533 **5.2 Results of observations**

534 The measurements were obtained on the University of Wyoming King Air aircraft during the
535 COPE-MED project in South-Western part of UK during July-August 2013 (Leon et al., 2016). The
536 UW King Air was equipped with a suite of microphysical instruments, including a DMT Cloud
537 Droplet probe (CDP), designed for measurements of droplet sizes and their concentrations in the
538 nominal size ranges 1–50 μm .

539 Figure 13 shows a time series of droplet concentration, extinction coefficient, liquid water
540 content and mean volume droplet diameter measured by the CDP during transit through a
541 convective cell on 18 July 2013. The CDP data were sampled at 10Hz, which corresponds to
542 approximately 10m spatial averaging. Visual examination of the spatial changes of N , β and LWC
543 shows strong correlation. The amplitude of changes of these parameters reaches nearly one hundred
544 percent with respect to their maximum. Contrary to that, the spatial variations of \bar{D} and D_v are quite
545 conservative and their values remain nearly constant. With the exception of two cloud holes

546 between 13:50:42 and 13:50:44, the amplitude of fluctuations of D_v does not exceed 8% with
547 standard deviation of 2.2%.

548 Figure 14 shows scatter diagrams of $LWC(N)$, $\beta(N)$, $LWC(\beta)$ and $D_v(N)$ measured by the
549 CDP during seven consecutive penetrations of the same convective cell extended over a period of
550 approximately 19 min. One of these penetrations is shown in Fig. 13. The measurements were
551 conducted at $H = 5500\text{m}$ and $T = -12^\circ\text{C}$. The relative humidity of the ambient air was approximately
552 20 %. At the beginning of the sampling no precipitation size particles were observed in the cloud.
553 However, by the end of the sampling period some raindrops and ice crystals were present in the
554 cloud. Despite the presence of some precipitation size particles, the scatter diagrams in Fig. 14a, b
555 and d demonstrate high correlation between pairs N , β and LWC . The mean volume diameter in
556 Fig. 14c shows very little changes from 19 to 17 μm when concentration changes from 1100 to 500
557 cm^{-3} , However, for $N < 200 \text{ cm}^{-3}$, the volume diameter decreases to 12–15 μm .

558 Red lines in Fig. 14 indicate $q(N)$, $\beta(N)$, $LWC(\beta)$ and $D_v(N)$ calculated for the 1st stage of
559 homogeneous mixing. The calculations were performed for a monodisperse $f(D)$ with $D_1=18.5\mu\text{m}$,
560 $N_1 = 1100 \text{ cm}^{-3}$, and state parameters as during the measurements. Comparisons of dependences
561 $q(N)$, $\beta(N)$, $LWC(\beta)$ and $D_v(N)$ based on in-situ measurements with those obtained from
562 numerical simulations of homogeneous mixing show minor difference for high concentrations 700
563 $\text{cm}^{-3} < N < 1100 \text{ cm}^{-3}$ (Fig. 14a–c). Simulation also shows that for this specific case the difference
564 between homogeneous and inhomogeneous mixing does not exceed 10% when $700 \text{ cm}^{-3} < N <$
565 1100 cm^{-3} . Such difference remains within the errors of measurements. Therefore, in this specific
566 cloud for the regions with $N > 700 \text{ cm}^{-3}$ the type of mixing cannot be unambiguously identified
567 from the analysis of the dependences $LWC(N)$, $\beta(N)$, $LWC(\beta)$ and $D_v(N)$. This is consistent with
568 the assessment of feasibility of segregation of homogeneous and inhomogeneous mixing in Fig.3
569 (dashed line). Since for homogeneous mixing $N \propto \mu$, than Fig.3 suggests good separation of the
570 moments for $N > 700 \text{ cm}^{-3}$.

571 For the regions with $N < 500 \text{ cm}^{-3}$ the deviation between homogeneous mixing simulations
572 and in-situ measurements in Fig.14 becomes well pronounced and it extends beyond possible errors
573 of measurements. This suggests that the mixing in these regions is dominated by the **extreme**
574 **inhomogeneous** type.

575 Figure 15 shows the same type of diagrams as in Fig. 14, which were measured during 45
576 consecutive traverses through an ensemble of deep convective cells. The sampling altitude varied

577 in the range $3000\text{m} < H < 4500\text{m}$, temperature $-11^\circ\text{C} < T < 0^\circ\text{C}$, relative humidity in the vicinity of
578 clouds $15\% < \text{RH} < 65\%$. The cloud measurements were extended over a period of 2 h 13 m, which
579 is suggestive that the convective cells were sampled at different stages of their lifetime. At the
580 sampling level the concentration of raindrops varied from zero to few per liter, and their diameter
581 did not exceed 2mm.

582 What is interesting that the scattering of the measurements $LWC(N)$, $\beta(N)$ and $LWC(\beta)$ (Fig.
583 15a, b and d) is limited by the sector, which originates from the zero point as in Fig.12a. Analysis
584 of the measurements showed that the data points $LWC(N)$, $\beta(N)$, $LWC(\beta)$ in each individual cloud
585 traverse are well aligned along the lines with different slopes (e.g. Fig.14). After averaging over the
586 ensemble of clouds, the area of the scattered points turned out to be located inside a sector limited
587 by the lines with smallest and largest slopes.

588 Comparisons of the scatterdiagrams $LWC(N)$, $\beta(N)$ and $LWC(\beta)$ in Figs.14 and 15 with the
589 conceptual diagrams in Fig.12 unambiguously suggest that interaction between cloud and
590 environment in the studied clouds was dominated by inhomogeneous mixing. It should be
591 emphasized that analysis of a stand alone mixing diagram $N - D_v$ would not allow unambiguously
592 draw such conclusion.

593

594 **6. Discussion**

595 One of the assumptions in most past studies is that for a sequence of the cloud samples collected
596 along the flight path, the adiabatic values of N_1 , q_1 , β_1 , D_1 and environmental parameters e_2 and T_2
597 remain the same. In fact these parameters may vary both within the same cloud or sequence of
598 samples clouds, and the amplitude of their variations depends on microphysical and
599 thermodynamical properties inside and outside the cloud environment. This variation will result in
600 an ensemble of relationships $M_n = F_{nk}(M_k)$, and enhance scattering of the data points. In such
601 cases identification of the type of mixing based on the $N - D_v$ diagram may result in confusion
602 between homogeneous and inhomogeneous mixing. As demonstrated in Sect. 5, consideration of
603 $N - q$ and $N - \beta$ diagrams may provide a better identification type of mixing.

604 **Strictly speaking the identification of type of mixing from particle probe measurements as it**
605 **was performed in Sect. 5 is incomplete. It allows establishing correlation between microphysical**
606 **moments and makes a formal conclusion about the mixing type, however it does not allow**
607 **judgement about stage of mixing (i.e. whether mixing is complete by reaching equilibrium). In most**

608 previous studies, including this one, identification of type of mixing was based on the assumption
609 that the sampled cloud volume is in equilibrium state ($RH = 1$), and that it reached the final stage
610 of mixing (Fig.1 a2, a3, b3). It is possible that at the moment of measurement the process of mixing
611 is not complete and the droplet free filaments remained undersaturated (Fig.1 a1, b1, b2). In this
612 case the relationship between different moments may be well described as $M_n = \alpha_{nk} M_{nk}$ and the
613 mixing be confused with inhomogeneous mixing.

614 In order to identify stage of mixing, high frequency collocated measurements of temperature
615 and humidity are required. Unfortunately current technology does not allow such measurements
616 yet.

617 Identification of type of mixing from in-situ observations is based on examination of
618 relationships between moments of the size distributions measured along the flight path. The basic
619 assumption underlying this analysis is that the cloud environment is not affected by other non-
620 adiabatic processes.

621 Thus, collision-coalescence, riming or Wegener-Bergeron-Findeisen processes may change the
622 droplet number concentration and liquid water content, and therefore, affect the relationship
623 between the moments. Activation of interstitial CCN will result in breaking correlation between the
624 moments due to formation of large concentration of droplets. Broad size distributions may also
625 hinder identification of type of mixing due to partial evaporation of small droplets (Pinsky et al.
626 2016a)

627 It is anticipated that most suitable candidates to study mixing-entrainment process are non-
628 precipitating convective clouds and stratocumulus clouds with relatively narrow droplet size
629 distributions.

630 Another limiting factor is that the above consideration did not account for the effect of changing
631 humidity in a vertically ascending parcel. Thus in droplet free entrained air relative humidity
632 increases approximately 10% for $\Delta z = 200\text{m}$ at $T = 0^\circ\text{C}$. After reaching saturation the mixing turns
633 into a degenerate case, which will appear as extreme inhomogeneous mixing. Joint effects of
634 evaporating droplets and an increase in S during the vertical ascent may facilitate reaching
635 saturation state. This case may also be relevant to the convective cloud described in Sect.5.2.

636
637
638

7. Conclusions

This study analyzes dependences of different moments of $f(D)$ in the frame of formalism of homogeneous and extremely inhomogeneous mixing. The analysis was performed for the final stage of mixing based on the mass and energy conservation consideration. The following results were obtained in the frame of this study:

1. Simple analytical relationships between the main microphysical moments were obtained for the final state homogenous and **extreme inhomogeneous** mixing.

2. It was shown that the functional relationships between the moments exist only for the first stage of homogeneous mixing, when equilibrium is reached. Subsequent progressive homogeneous mixing breaks the functional relationship between the moments.

3. It was demonstrated that consideration of scattering $N - LWC$, $N - \beta$ diagrams facilitates identification of type of mixing from in-situ measurements. For **extreme inhomogeneous** mixing the scattering of the data points $N - LWC$, $N - \beta$ will be limited by a sector originating at zero point (Fig.12a). However, for homogeneous mixing the scattering data points will be limited by a sector originating at (N_1, LWC_1) and (N_1, β_1) (Fig.12b). Utilizing a stand-alone conventional $N - D_v$ mixing diagram may not provide unambiguous answer about type of mixing.

4. The developed approach was applied to a set of in-situ measurements collected in convective clouds. The analysis of the dependences between N , β , LWC and D_v suggests that the interaction between entrained and cloudy environments for the studied clouds was dominated by inhomogeneous mixing.

The present study considers relationships between different moments of $f(D)$ for the final stage of mixing. The following two works Pinsky et al. (2016a, b) in this series provide a detailed analysis of time dependences of droplet size distributions and its moments during homogeneous and inhomogeneous mixing.

Acknowledgement. The authors appreciate two anonymous reviewers for their comments. Alexei Korolev work was supported by Environment Canada and Transport Canada. The COPE-MED project was funded by National Science Foundation grant AGS-1230292 and AGS-1230203. The contribution of Mark Pinsky and Alex Khain was supported by the Israel Science Foundation (grant 1393/14), the Office of Science (BER), US Department of Energy Award DE-SC0006788 and the Binational US-Israel Science foundation (grant 2010446).

670

671 **Appendix A: Liquid water deficit**

672 The objective of this section is to find the amount of liquid water, which is required to be
 673 evaporated in order to saturate the parcel formed after mixing. Assume that q_{v1} , q_{v2} are the mixing
 674 vapor ratios in the cloudy and entrained parcels, respectively, and T_1 , T_2 are their respective initial
 675 temperatures. First, we find the saturation ratio S_{m0} formed after instant mixing of the cloud and
 676 entrained before the cloud droplets start evaporating.

677 The vapor mixing ratio q_{vm} formed in the mixed volume will be

$$678 \quad q_{vm} = \mu q_{v1} + (1 - \mu) q_{v2} \quad (\text{A1})$$

679 The vapor pressure e_m in the mixed volume can be derived from Eq. (A1) by substituting

$$680 \quad q_v = \frac{e}{p - e} \frac{R_a}{R_v}, \text{ i.e.}$$

$$681 \quad e_m = p \frac{\mu + \frac{e_2(p - e_1)}{p(e_1 - e_2)}}{\mu + \frac{(p - e_1)}{(e_1 - e_2)}} \quad (\text{A2})$$

682 The temperature of the mixed volume T_{m0} can be found from the energy conservation law

$$683 \quad \mu(q_{v1}c_{pv} + c_{pa})(T_1 - T_{m0}) = (1 - \mu)(q_{v2}c_{pv} + c_{pa})(T_{m0} - T_2) \quad (\text{A3})$$

684 here c_{pv} , c_{pa} , are the specific heat capacitance of water vapor and dry air at constant pressure,
 685 respectively, T_1 , T_2 are the initial temperatures in the first and second parcels before mixing.
 686 Substituting q_{v1} , q_{v2} yields the temperature in the mixed volume

$$687 \quad T_{m0} = \frac{\mu T_1 + \alpha(1 - \mu)T_2}{\mu + \alpha(1 - \mu)} \quad (\text{A4})$$

688 here

$$689 \quad \alpha = \frac{1 + \frac{c_{pv}R_a e_2}{c_{pa}R_v(p - e_2)}}{1 + \frac{c_{pv}R_a e_1}{c_{pa}R_v(p - e_1)}} \quad (\text{A5})$$

690 With a good accuracy $\alpha \cong 1$. The resulting relative humidity after mixing the two volumes will
 691 be

692
$$RH_{m0} = \frac{e_{m0}}{e_s(T_{m0})} \quad (A6)$$

693 where $e_s(T_{m0})$ is the saturated vapor pressure at temperature T_{m0} .

694 The process of evaporation is accompanied by changing humidity and temperature due to latent
 695 heat of vaporization. This process is described by the Eq. (C2) in Korolev and Mazin (2003).
 696 Assuming the process to be isobaric (i.e. vertical velocity $u_z = 0$) and absence of ice ($dq_i = 0$),
 697 Eq. (C2) (Korolev and Mazin, 2003) yields

698
$$\frac{dS}{S+1} = \left(\frac{1}{S+1} \frac{pR_v}{e_s R_a} + \frac{L^2}{c_{pa} R_v T^2} \right) dq \quad (A7)$$

699 Integrating Eq. (A7) from initial S_{m0} to saturation state, when $S = 0$, and taking into account
 700 that $RH = S + 1$, gives

701
$$\delta q_m = -b \ln \left(\frac{1 + aRH_{m0}}{1 + a} \right) \quad (A8)$$

702 the mixing ratio of liquid water required to evaporate in order to saturate 1kg of the cloud volume
 703 formed after mixing with the entrained air, but before droplet start evaporating. Here $a = \frac{E_s R_a L^2}{\rho c_p R_v^2 T_{m0}^2}$,

704
$$b = \frac{c_p R_v T_{m0}^2}{L^2}$$

705 Since $\left| \frac{A(RH_{m0}-1)}{1+A} \right| < 1$, Eq.(A8) can be simplified as

706
$$\delta q_m = ab \frac{1 - RH_{m0}}{1 + a} = -\frac{S_{m0}}{A_2} \quad (A9)$$

707 where $A_2 = \frac{ab}{1+a}$. The analysis of Eqs. (A8)-(9) shows that for wide range of temperatures $-30 \text{ }^\circ\text{C} <$
 708 $T < 30 \text{ }^\circ\text{C}$, both equations hold with high accuracy as long as the temperatures of the sub-saturated
 709 and cloud parcels $|T_1 - T_2| < 10^\circ\text{C}$.

710 Figure A1 shows comparisons of modeled δq_m and that calculated from Eqs. (A8) and (A9)
 711 for three different temperatures. The model solved a system of differential equation with
 712 incremental evaporation of liquid water until saturation is reached. As seen from Fig. A1 the
 713 agreement between modeled δq_m and that calculated from Eq. (A8)-(A9) is quite good and does
 714 not exceed few percent at $RH_{m0} = 0.5$. This discrepancy results from assumption that e_s and T are
 715 constant in Eqs.(A8)-(A9).

716

717 **Appendix B: Liquid water deficit when $T_1 = T_2$**

718 Eq.(A2) by assuming that $p \gg e_1$ and $p \gg e_2$ can be simplified as

719
$$e_{m0} = \mu e_1 + (1 - \mu)e_2 \quad (B2)$$

720 As follows from Eq.(A4) for the case $T_1 = T_2$ with high accuracy $T_{m0} = T_1 = T_2$. Therefore,
721 $e_s(T_{m0}) = e_s(T_1) = e_s(T_2)$. Dividing Eq.(B1) by e_s yields

722
$$RH_{m0} = \mu RH_1 + (1 - \mu)RH_2 \quad (B3)$$

723 In most liquid clouds $RH_1 = 1$ (Korolev and Mazin 2003). Therefore, Eq.B2 turns into

724
$$RH_{m0} = \mu + (1 - \mu)RH_2 \quad (B4)$$

725 Substituting Eq.(B4) in Eq.(B1) yields

726
$$\delta q_m = -b \ln \left(1 + \frac{a(1 - \mu)(RH_2 - 1)}{1 + a} \right) \quad (B5)$$

727 The expression under logarithm can be presented as the first two terms of the series expansion
728 of $\left(1 + \frac{a(RH_2 - 1)}{1 + a} \right)^{(1 - \mu)}$. Substituting this expression into Eq.(B5), gives

729
$$\delta q_m = (1 - \mu)\delta q^* \quad (B6)$$

730 where

731
$$\delta q^* = -b \ln \left(\frac{1 + aRH_2}{1 + a} \right) \quad (B7)$$

732 is the mixing ratio of liquid water required to saturate 1 kg of the entrained dry volume.

733

734 **Appendix C: Temperature in the mixing volume**

735 The energy conservation for evaporating droplets can be written as

736
$$(T - T_{m0})(1 + q_{vm})c_{pm} + (1 - \mu)\delta q^* L = 0 \quad (C1)$$

737 here c_{pm} is the specific heat capacity of the moist air

738
$$c_{pm} = \frac{c_{pa} + q_{vm}c_{pv}}{1 + q_{vm}} \quad (C2)$$

739 Since $q_{vm} \ll 1$ and, $c_{pa} \cong c_{pm}$ Eq.(C1) may be simplified, so that the final temperature after
740 mixing

741
$$T = T_{m0} - \frac{(1 - \mu)\delta q^* L}{c_{pa}} \quad (C3)$$

742 For the case when $T_1 \neq T_2$ Eq. (C3) should be replaced by

$$743 \quad T = T_{m0} - \frac{\delta q_m L}{c_{pa}} \quad (C4)$$

744 Eqs. (C3) and (C4) are valid for the mixing fraction $\mu > \mu_{cr}$. For $\mu \leq \mu_{cr}$ all entrained liquid
745 water μq_0 evaporates, and the final temperature will be

$$746 \quad T = T_{m0} - \frac{\mu q_0 L}{c_{pa}} \quad (C5)$$

747

748 **References**

- 749 Andrejczuk M., Grabowski, W. W., Malinowski, S. P., and Smolarkiewicz, P. K.: Numerical
750 simulation of cloud–clear air interfacial mixing: homogeneous vs. inhomogeneous mixing., J.
751 Atmos. Sci., 66, 2493-2500, 2009.
- 752 Baker, M. B. and Latham, J.: The evolution of droplet spectra and the rate of production of
753 embryonic raindrops in small cumulus clouds, J. Atmos. Sci., 36, 1612–1615, 1979.
- 754 Baker, M. B. and Latham, J.: A diffusive model of the turbulent mixing of dry and cloudy air, Q. J.
755 R. Met. Soc., 108, 871–898, 1982.
- 756 Baker, M. B., Corbin, R. G., and Latham, J.: The influence of entrainment on the evolution of cloud
757 droplet spectra: I. A model of inhomogeneous mixing, Q. J. Roy. Meteor. Soc., 106, 581–598,
758 1980.
- 759 Beals, M.J., and Fugal, J.P., Shaw, R.A., Lu, J., Spuler, S.M., Stith, J.L.: Holographic measurements
760 of inhomogeneous cloud mixing at the centimeter scale. Science, 350, 87-90, 2015
- 761 Bohren, C. F. and Albrecht, C. H.: Atmospheric Thermodynamics, Oxford University Press, New
762 York, 402 pp., 1998.
- 763 Bower, K. N. and Choulaton, T. W.: The effects of entrainment on the growth of droplets in
764 continental cumulus clouds, Q. J. Roy. Meteor. Soc., 114, 1411–1434, 1988.
- 765 Broadwell, J. E., and R. E. Breidenthal: A simple model of mixing and chemical reaction in a
766 turbulent shear layer. J. Fluid Mech., 125, 397–410, 1982
- 767 Burnet, F. and Brenguier, J. L.: Observational study of the entrainment-mixing process in warm
768 convective clouds, J. Atmos. Sci., 64, 1995–2011, 2007.

769 Devenish, B. J., Bartello, P., Brenguier, J.-L., Collins, L. R., Grabowski, W. W., Ijzermans, R. H.
770 A., Malinovski, S. P., Reeks, M.W., Vassilicos, J. C., Wang, L- P., and Warhaft, Z.: Droplet
771 growth in warm turbulent clouds, *Q. J. Roy. Meteor. Soc.*, 138, 1401–1429, 2012.

772 Dimotakis, P. E.: Turbulent mixing, *Annu. Rev. Fluid Mech.*, 37, 329–356, 2005.

773 Gerber, H., Frick, G., Jensen, J. B., and Hudson, J. G.: Entrainment, mixing, and microphysics in
774 trade-wind cumulus, *J. Meteorol. Soc. Jpn.*, 86, 87–106, 2008.

775 Hill, T. A. and Choulaton, T. W.: An airborne study of the microphysical structure of cumulus
776 clouds, *Q. J. Roy. Meteor. Soc.*, 111, 517–544, 1985.

777 Jeffery, C. A.: Inhomogeneous cloud evaporation, invariance, and Damköhler number, *J. Geoph.*
778 *Res.*, 112, D24S21, doi:10.1029/2007JD008789, 2007.

779 Jarecka, D., Grabowski, W. W., Morrison, H., Pawlowska, H.: Homogeneity of the Subgrid-Scale
780 Turbulent Mixing in Large-Eddy Simulation of Shallow Convection. *J. Atmos. Sci.* 70, 2751-
781 2767, 2013

782 Jensen, J. and Baker, M.: A simple model of droplet spectra evolution during turbulent mixing, *J.*
783 *Atmos. Sci.*, 46, 2812–2829, 1989.

784 Korolev A. V.: The influence of supersaturation fluctuations on droplet spectra formation. *Journal*
785 *of the Atmospheric Sciences*, 52, 3620-3634, 1995.

786 Korolev, A. V. and Isaac, G. A.: Drop growth due to high supersaturation caused by isobaric mixing,
787 *J. Atmos. Sci.*, 57, 1675–1685, 2000.

788 Korolev, A. V. and I.P. Mazin,: Supersaturation of water vapor in clouds. *J. Atmos. Sci.*, 60, 2957-
789 2974, 2003.

790 Krueger, S., Su, C.-W., and McMurtry, P.: Modeling entrainment and finescale mixing in cumulus
791 clouds, *J. Atmos. Sci.*, 54, 2697–2712, 1997.

792 Kumar, B., Schumacher, J., and Shaw, R. A.: Cloud microphysical effects of turbulent mixing and
793 entrainment, *Theor. Comput. Fluid Dyn.*, 27, 361–376, 2013.

794 Lasher-Trapp, S. G., Cooper, W. A., and Blyth, A. M.: Broadening of droplet size distributions
795 from entrainment and mixing in a cumulus cloud, *Q. J. Roy. Meteor. Soc.*, 131, 195–220, 2005.

796 Latham, J. and Reed, R. L.: Laboratory studies of the effects of mixing on the evolution of cloud
797 droplet spectra, *Q. J. Roy. Meteor. Soc.*, 103, 297–306, 1977.

798 Lehmann, K., Siebert, H., and Shaw, R. A.: Homogeneous and inhomogeneous mixing in cumulus
799 clouds: dependence on local turbulence structure, *J. Atmos. Sci.*, 66, 3641–3659, 2009.

800 Leon, D. C., French, J. R., Lasher-Trapp, S., Blyth, A. M., Abel, S. J., Ballard, S., Bennett, L. J.,
801 Bower, K., Brooks, B., Brown, P., Choullarton, T., Clark, P., Collier, C., Crosier, J., Cui, Z.,
802 Dufton, D., Eagle, C., Flynn, M. J., Gallagher, M., Hanley, K., Huang, Y., Kitchen, M., Korolev,
803 A., Lean, H., Liu, Z., Marsham, J., Moser, D., Nicol, J., Norton, E. G., Plummer, D. Price, J.,
804 Ricketts, H., Roberts, N., Rosenberg, P. D., Taylor, J. W., Williams, P. I., and Young, G.: The
805 Convective Precipitation Experiment (COPE): investigating the origins of heavy precipitation in
806 the southwestern UK, *B. Am. Meteorol. Soc.*, in press, 2016.

807 Lu, C., and Liu Y., Niu, S.: Examination of turbulent entrainment mixing mechanisms using a
808 combined approach. *J. Geoph. Res.*, 116, D20207, 2011.

809 Paluch, I. R.: Mixing and the droplet size spectrum: generalizations from the CCOPE data, *J. Atmos.*
810 *Sci.*, 43, 1984–1993, 1986.

811 Paluch, I. R. and Baumgardner, D. G.: Entrainment and fine-scale mixing in a continental
812 convective cloud, *J. Atmos. Sci.*, 46, 261–278, 1989.

813 Paluch, I. R. and Knight, C. A.: Mixing and evolution of cloud droplet size spectra in a vigorous
814 continental cumulus, *J. Atmos. Sci.*, 41, 1801–1815, 1984.

815 Pinsky, M., Khain, A., Korolev, A., and Magaritz-Ronen, L.: Theoretical investigation of mixing
816 in warm clouds – Part 2: Homogeneous mixing, *Atmos. Chem. Phys. Discuss.*, 15, 30269-30320,
817 doi:10.5194/acpd-15-30269-2015, 2015.

818 Pinsky, M., Khain, A., and Korolev, A.: Theoretical analysis of mixing in liquid clouds – Part 3:
819 Inhomogeneous mixing, *Atmos. Chem. Phys. Discuss.*, 15, 30321–30381, doi:10.5194/acpd-15-
820 30321-2015, 2015.

821 Rogers, R. R.: *A Short Course in Cloud Physics*, Pergamon press, Oxford, 227 pp., 1976.

822 Squires, P.: The growth of cloud drops by condensation. *Aust. J. Sci. Res.*, 5, 66–86, 1952.

823 Su, C.-W., Krueger, S. K., McMurtry, P. A., and Austin, P. H.: Linear eddy modeling of droplet
824 spectral evolution during entrainment and mixing in cumulus clouds, *Atmos. Res.*, 47-48, 41-
825 58, 1998.

826 **Table 1**827 **List of Symbols**

Symbol	Description	Units
A_2	$\frac{pR_v}{e_s R_a} + \frac{L^2}{c_{pa} R_v T^2}$	-
a	$\frac{e_s R_a L^2}{p c_{pa} R_v T^2}$	-
b	$\frac{c_{pa} R_v T^2}{L^2}$	-
c_{pa}	specific heat capacity of dry air at constant pressure	$\text{J kg}^{-1}\text{K}^{-1}$
c_{pv}	specific heat capacity of water vapor at constant pressure	$\text{J kg}^{-1}\text{K}^{-1}$
\bar{D}	mean droplet diameter	m
D_2	mean square droplet diameter	m
D_v	mean volume droplet diameter	m
e	water vapor pressure	N m^{-2}
e_1	initial water vapor pressure in the cloud parcel	N m^{-2}
e_2	initial water vapor pressure in the entrained sub-saturated parcel	N m^{-2}
e_s	saturation vapor pressure above flat surface of water	N m^{-2}
$f(D)$	size distribution of cloud droplets normalized on unity	m^{-1}
L	latent heat for liquid water	J kg^{-1}
M_n	n -th moment of the droplet size distribution	$\frac{\int_0^{\infty} f(r)r^n dr}{\int_0^{\infty} f(r)dr}$ m^n
N	concentration of droplets	m^{-3}
N_1	concentration of droplets before mixing	m^{-3}
p	pressure of moist air	N m^{-2}
R_a	specific gas constant of moist air	$\text{J kg}^{-1}\text{K}^{-1}$
R_v	specific gas constant of water vapor	$\text{J kg}^{-1}\text{K}^{-1}$
RH	e/E_s , relative humidity over water (saturation ratio)	-

RH_1	initial relative humidity in the cloud volume ($RH_1=1$)	-
RH_2	relative humidity in the entrained sub-saturated parcel	-
RH_{m0}	relative humidity after instant mixing of cloudy and entrained air but before droplets evaporation	-
q	cloud liquid water mixing ratio (mass of liquid water per 1kg of dry air)	-
q_1	cloud liquid water mixing ratio before mixing	-
q_v	water vapor mixing ratio (mass of water vapor per 1kg of dry air)	-
S	$e/e_s - 1$, supersaturation	-
S_2	supersaturation of the dry out-of-cloud air	-
S_{m0}	supersaturation after instant mixing of cloudy and entrained air, but before droplets start evaporating	-
T	temperature	K
T_1	temperature of the cloud parcel before mixing	K
T_2	temperature of the entrained sub-saturated parcel before mixing	K
T_{m0}	temperature of the parcel after vapor mixing, but before droplet evaporation	K
β	extinction coefficient	m^{-1}
β_1	extinction coefficient before mixing	m^{-1}
δq_m	mixing ratio of liquid water required to saturate 1kg of the cloud volume after instant mixing, but before droplet evaporation.	-
δq^*	mixing ratio of liquid water required to saturate 1kg of the dry out-of-cloud air	-
μ	cloud fraction of mixing air, $0 \leq \mu \leq 1$	-
μ_{cr}	critical cloud fraction, such that for $\mu \leq \mu_{cr}$ all droplets evaporate	-
ρ_a	density of the dry air	$kg\ m^{-3}$
ρ_w	density of liquid water	$kg\ m^{-3}$
ξ	coefficient $0 \leq \xi \leq 1$ characterizing proximity of homogeneous mixing to inhomogeneous (when $\xi \rightarrow 0$).	-

829 **Figure Captions**

830 **Figure 1.** Classical conceptual diagram of (a) inhomogeneous and (b) homogeneous mixing. 1
831 initial state; 2 mixing state; 3 final state.

832 **Figure 2.** Dependence of critical mixing fraction μ_{cr} versus mixing ratio q_0 calculated from Eq.(7).
833 Circles indicate modeled points. The calculations were performed for $T=0C$ and
834 $H=3000m$.

835 **Figure 3.** Dependence of ξ versus μ . Numbers are the dimensionless ratios $\delta q^*/q_1$. Critical mixing
836 ratios μ_{cr} are indicated by stars. Grey area indicates area where the moments of
837 homogeneous and **extreme inhomogeneous** mixing may not be segregated from in-situ
838 measurements. Dashed line was calculated for the cloud in Figs.13-14.

839 **Figure 4.** Simulation of (a) liquid water mixing ratio, (b) droplet number concentration, (c) integral
840 droplet diameter, (d) extinction coefficient, (e) mean volume diameter, (f) time of phase
841 relaxation, (g) relative humidity in the mixed volume before droplet evaporation RH_{m0}
842 and at the equilibrium state RH_m , (h) final temperature T_{m0} versus ratio of mixing μ formed
843 after homogeneous and **extreme inhomogeneous** mixing between dry and cloudy parcel
844 with monodisperse droplets. Black stars indicate critical mixing fraction μ_{cr} calculated
845 from Eq.(7). The calculations were performed for $RH_2 = 0.2, 0.5, 0.8, 0.95$; $D_1=20\mu m$,
846 $N_1=500cm^{-3}$; $T_1 = T_2 = 0C$; $H=1000m$.

847 **Figure 5.** Dependence of normalized liquid water mixing ratio q/q_1 (a,d,g), extinction coefficient
848 β/β_1 (b,e,h) and mean volume diameter D_v/D_{v1} (c,f,j) versus normalized number
849 concentration N/N_1 for various humidity of the entrained air (a,b,c), for various liquid
850 water mixing ratios (d,e,f) and for various temperatures (g,h,j). The calculations were
851 performed the initial conditions: $H=1000m$, $D_1=20\mu m$; for (a-c; g-j) $N_1=500cm^{-3}$; for (a-
852 f) $T_1 = T_2 = 0C$.

853 **Figure 6.** Simulation of (a) droplet number concentration and (b) liquid water mixing ratio, (c)
854 integral droplet diameter, (d) extinction coefficient, (e) mean volume diameter, (f) time of
855 phase relaxation, (g) relative humidity in the mixed volume before droplet evaporation
856 RH_{m0} and at the equilibrium state RH_m , (h) final temperature T_m versus ratio of mixing μ
857 formed after homogeneous and **extreme inhomogeneous** mixing between dry and cloudy

858 parcel with monodisperse droplets. The calculations were performed for $RH_2=0.9$;
859 $D_1=10\mu\text{m}$, $N_1=500\text{cm}^{-3}$; $T_1 = 0\text{C}$; $T_2 = -10\text{C}, -5\text{C}, 0\text{C}$; $H=1000\text{m}$.

860 **Figure 7.** Effect of temperature difference between cloud and entrained air on mixing. The
861 calculations were performed for initial temperatures T_2 : (1) -10C ; (2) -5C ; (3) 0C . Grey
862 circles indicate **extreme inhomogeneous** mixing on line 1 at the AB interval. The rest cases
863 on extremely inhomogeneous mixing are indicated by open circles. The initial conditions
864 used for the calculations were: $H=1000\text{m}$, $RH_2=90\%$; $D_1 = 10\mu\text{m}$, $N_1 = 500\text{cm}^{-3}$, $T_1=0\text{C}$.

865 **Figure 8.** Conceptual diagram of cascade mixing of the out-of-cloud entrained parcel with the
866 cloudy environment

867 **Figure 9.** Simulation of stochastic mixing corresponding to stages 1-4 as indicated in Fig.8. Solid
868 red lines indicate the normalized dependences q , β , D_v vs. N for the primary stage of
869 homogeneous mixing. Dashed red lines indicate the same dependences for inhomogeneous
870 mixing. The initial conditions used for the simulations were: $H=1000\text{m}$, $T_1 = T_2 = 0\text{C}$;
871 $RH_2=0.5$; $D_1 = 10\mu\text{m}$, $N_1 = 500\text{cm}^{-3}$.

872 **Figure 10.** Conceptual diagram explaining breaking the functional relationships between the
873 microphysical moment during progressive missing (see text).

874 **Figure 11.** Droplet size distributions formed during the progressive homogeneous mixing
875 corresponding to the (a,e) primary stage; (b,f) 2nd stage; (c,g) 3rd stage; (d,h) 4th stage. Left
876 column (a,b,c,d) corresponds to the case, when the cloud temperature is equal to the dry
877 air temperature $T_1 = T_2 = 0\text{C}$.; right column (e,f,g,h) corresponds to the case when $T_1 =$
878 0C , $T_2 = -10\text{C}$. For both cases the simulation was performed for $D_1 = 10\mu\text{m}$; $N=500\text{cm}^{-3}$;
879 $RH_2=0.9$.

880 **Figure 12.** Conceptual diagrams of scattering of measurements of q versus N for (a) **extreme**
881 **inhomogeneous** and (b) homogeneous mixing.

882 **Figure 13.** Spatial changes of particle concentration (a), extinction coefficient (b), liquid water
883 content (c) and average and mean mass diameter (d) during transit through one of the
884 convective clouds measured by CDP. The measurements were conducted during the
885 COPE-MED project on 18 July, 2015. The sampling rate 10Hz ($\sim 10\text{m}$ spatial resolution).
886 $H=5500\text{m}$, $T=-12\text{C}$, $RH=0.2$.

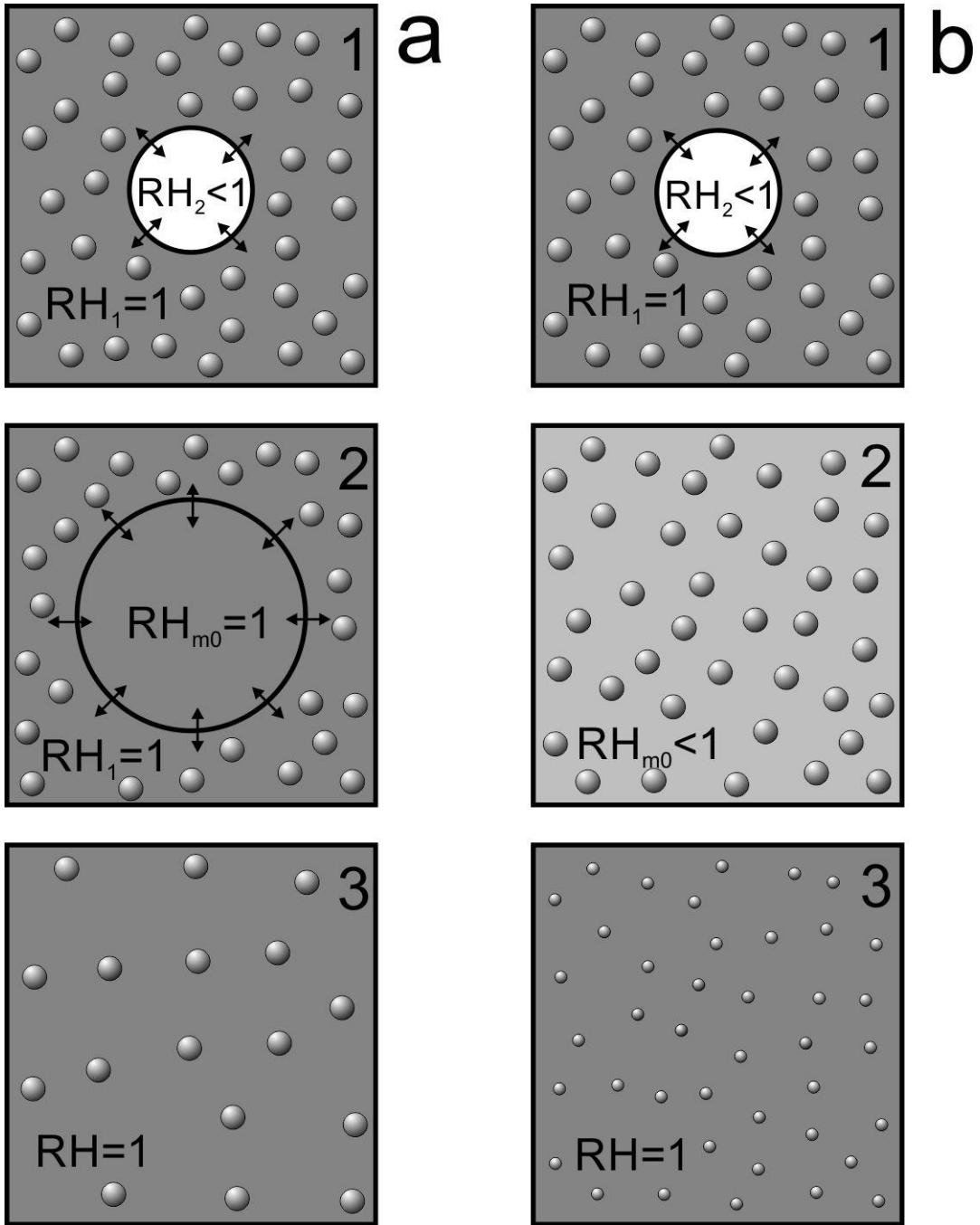
887 **Figure 14.** Relationships between (a) $LWC(N)$; (b) $\beta(N)$; (c) $D_v(N)$; (d) $LWC(\beta)$ calculated from
888 the CDP measurements obtained during sampling several convective clouds. The

889 measurements were conducted during the COPE-MED project on 18 July, 2015,
890 $H=5500\text{m}$, $T=-12\text{C}$, $RH=0.2$. The measurements were sampled at 10Hz (~10m spatial
891 resolution). Dashed lines are linear regressions. Red lines indicate primary inhomogeneous
892 mixing dependencies calculated for the same environmental conditions.

893 **Figure 15.** Relationships between (a) $LWC(N)$; (b) $\beta(N)$; (c) $D_v(N)$; (d) $LWC(\beta)$ calculated from
894 the CDP measurements sampled during traverse through 45 convective clouds. The
895 measurements were conducted during the COPE-MED project on 02 August, 2015.
896 Dashed lines indicate (a), (b) and (d) indicate the sectors, where the majority of the points
897 are scattered. The altitude of sampling varied in the range $3000\text{m} < H < 4500\text{m}$, temperature
898 $-11\text{C} < T < 0\text{C}$, relative humidity in the vicinity of clouds $15\% < RH < 65\%$. The measurements
899 were sampled at 10Hz (~10m spatial resolution).

900 **Figure A1.** Amount of evaporated liquid water δq_m required for saturation of a cloud volume with
901 initial humidity RH_m . Comparisons of the modeled δq_m and that calculated from Eqs.
902 (A8) and (A9) for three temperatures $T_{m0} = -20\text{C}$, 0C and 20C . Calculations were
903 performed for $P=880\text{mb}$.

904



905

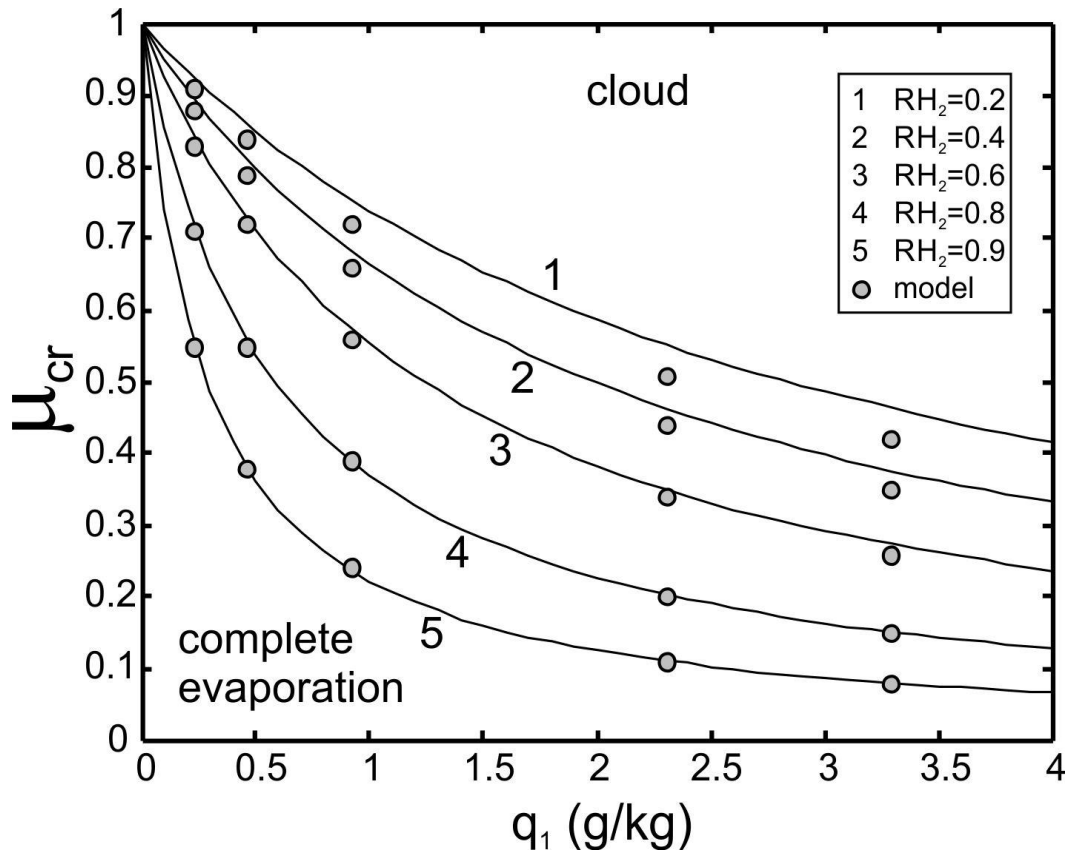
906

907 **Figure 1.** Classical conceptual diagram of (a) inhomogeneous and (b) homogeneous mixing. 1 initial state; 2 mixing

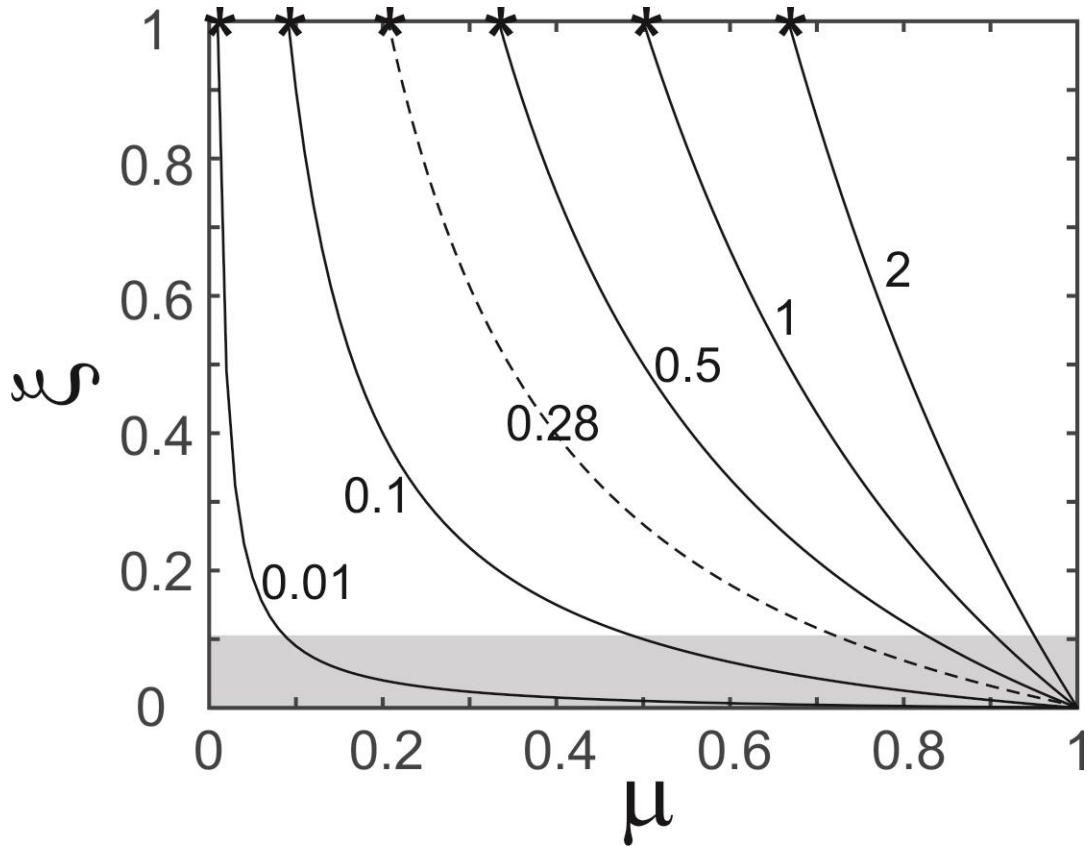
908 state; 3 final state.

909

910

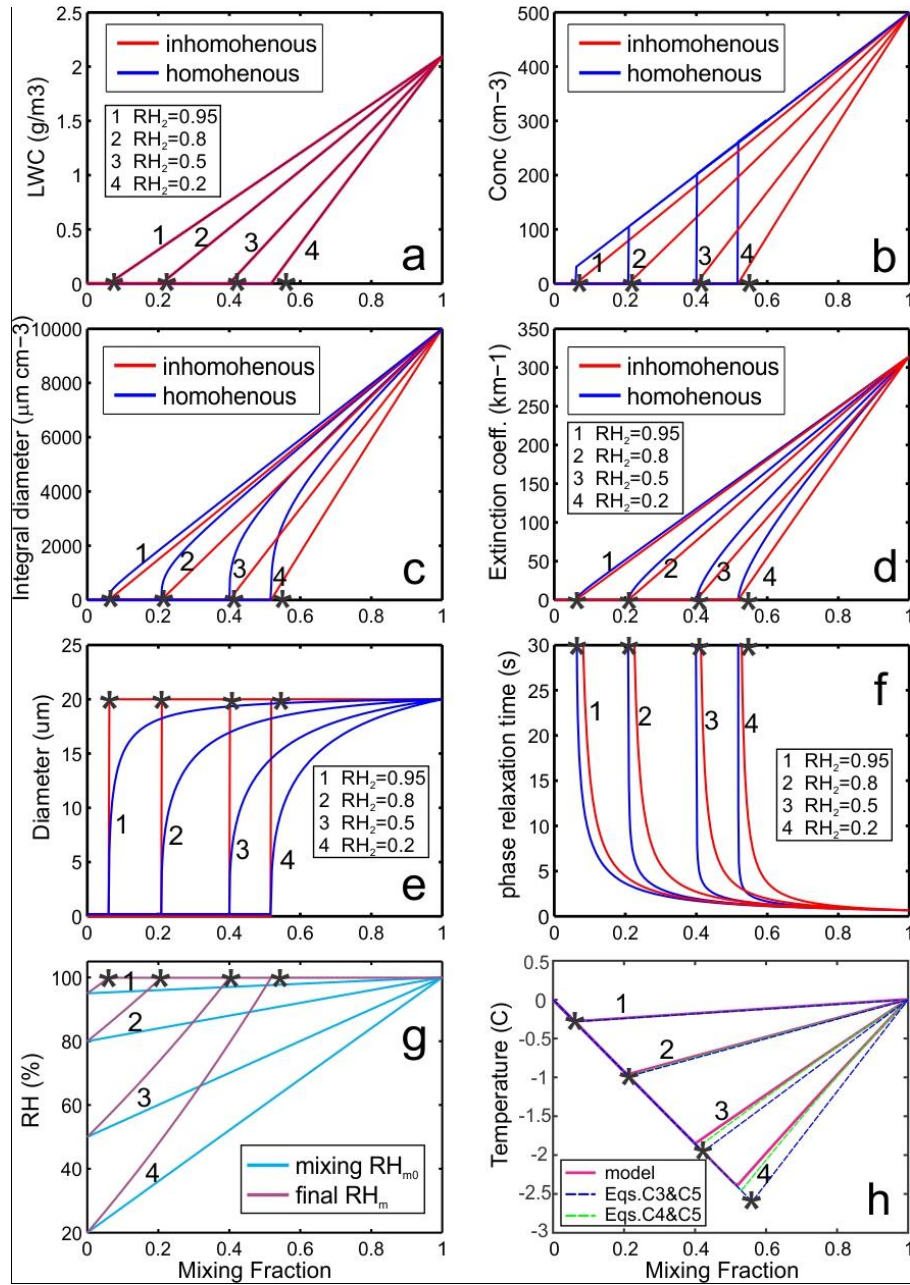


1
 2 **Figure 2.** Dependence of critical mixing fraction μ_{cr} versus mixing ratio q_0 calculated from Eq.(7). Circles indicate
 3 modeled points. The calculations were performed for $T=0C$ and $H=3000m$.
 4



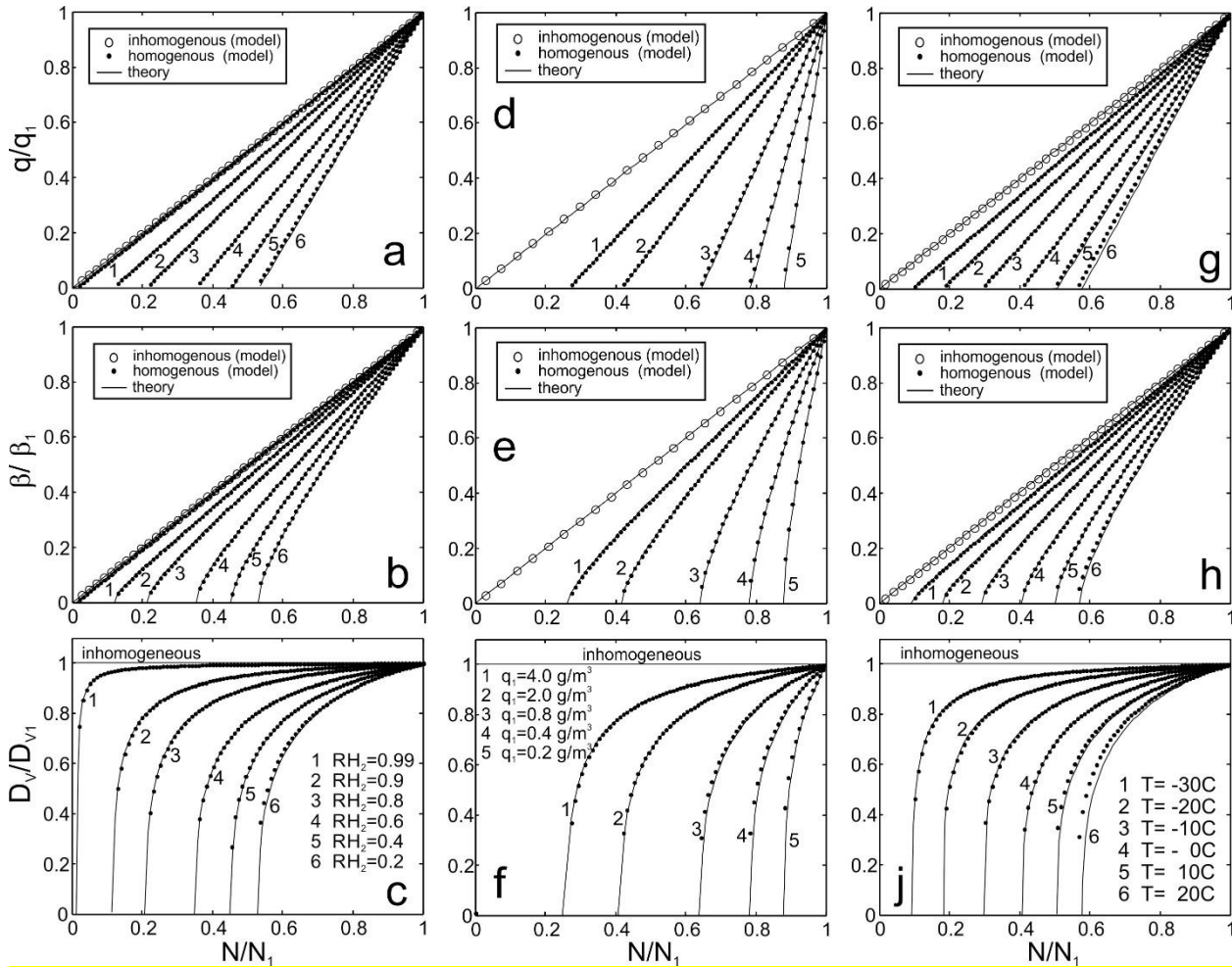
1
2
3
4
5
6

Figure 3. Dependence of ξ versus μ . Numbers are the dimensionless ratios $\delta q^*/q_1$. Critical mixing ratios μ_{cr} are indicated by stars. Grey area indicates area where the moments of homogeneous and extreme inhomogeneous mixing may not be segregated from in-situ measurements. Dashed line was calculated for the cloud in Figs.13-14.



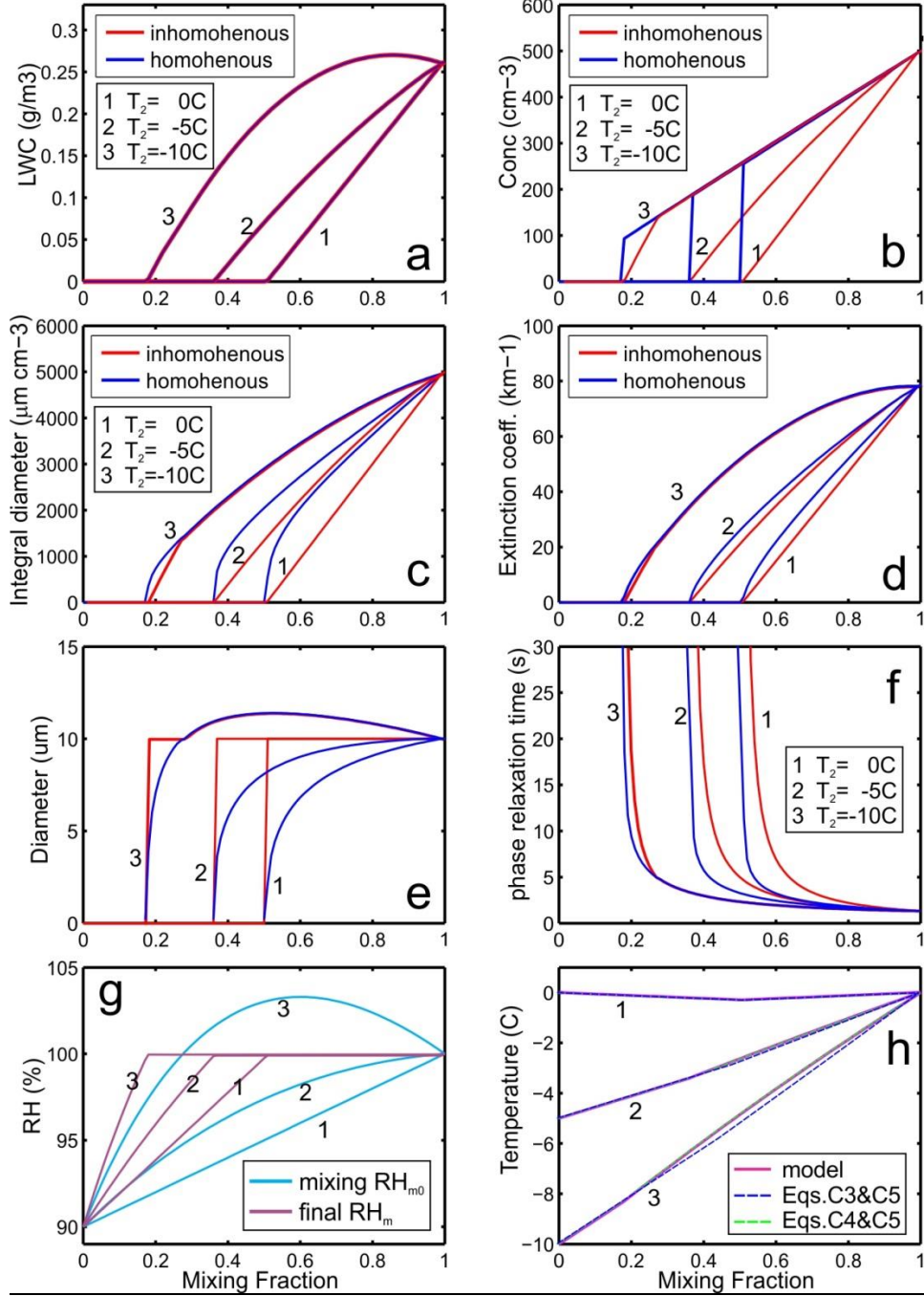
1
2

3 **Figure 4.** Simulation of (a) liquid water mixing ratio, (b) droplet number concentration, (c) integral droplet diameter,
 4 (d) extinction coefficient, (e) mean volume diameter, (f) time of phase relaxation, (g) relative humidity in the mixed
 5 volume before droplet evaporation RH_{m0} and at the equilibrium state RH_m , (h) final temperature T_{m0} versus ratio of
 6 mixing μ formed after homogeneous and extreme inhomogeneous mixing between dry and cloudy parcel with
 7 monodisperse droplets. Black stars indicate critical mixing fraction μ_{cr} calculated from Eq.(7). The calculations
 8 were performed for $RH_2 = 0.2, 0.5, 0.8, 0.95$; $D_1 = 20\mu\text{m}$, $N_1 = 500\text{cm}^{-3}$; $T_1 = T_2 = 0\text{C}$; $H = 1000\text{m}$.



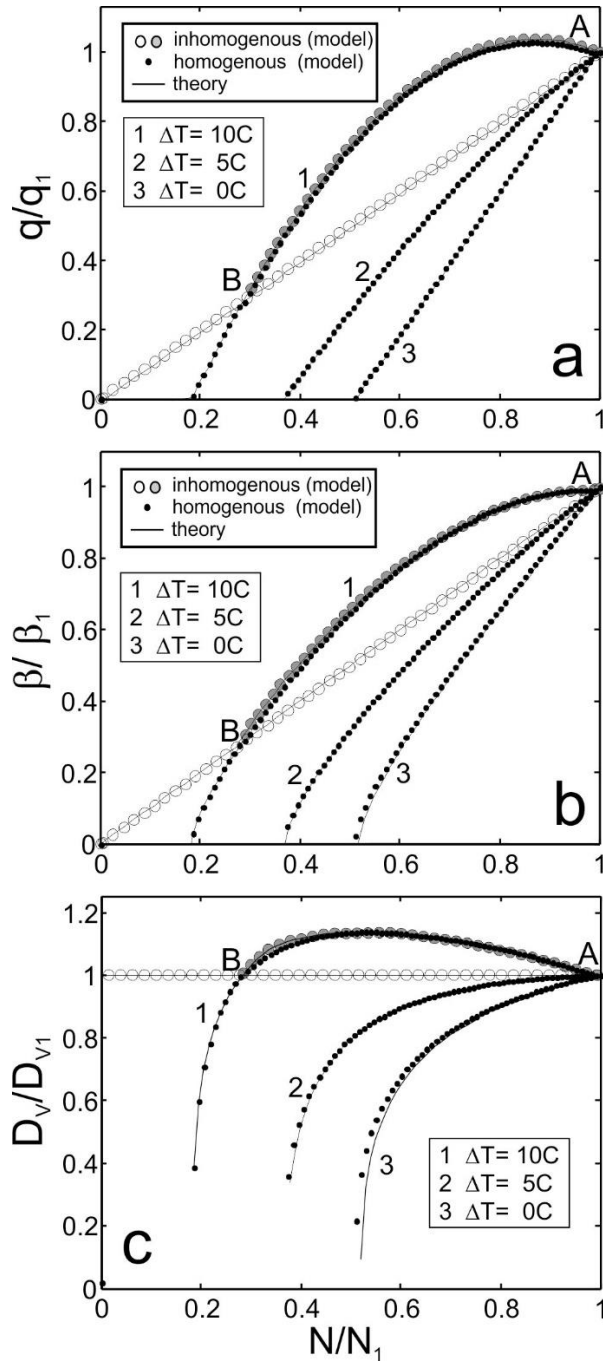
1
2
3
4
5
6
7

Figure 5. Dependence of normalized liquid water mixing ratio q/q_1 (a,d,g), extinction coefficient β/β_1 (b,e,h) and mean volume diameter D_v/D_{v1} (c,f,j) versus normalized number concentration N/N_1 for various humidity of the entrained air (a,b,c), for various liquid water mixing ratios (d,e,f) and for various temperatures (g,h,j). The calculations were performed the initial conditions: $H=1000\text{m}$, $D_1=20\mu\text{m}$; for (a-c; g-j) $N_1=500\text{cm}^{-3}$; for (a-f) $T_1 = T_2 = 0\text{C}$.



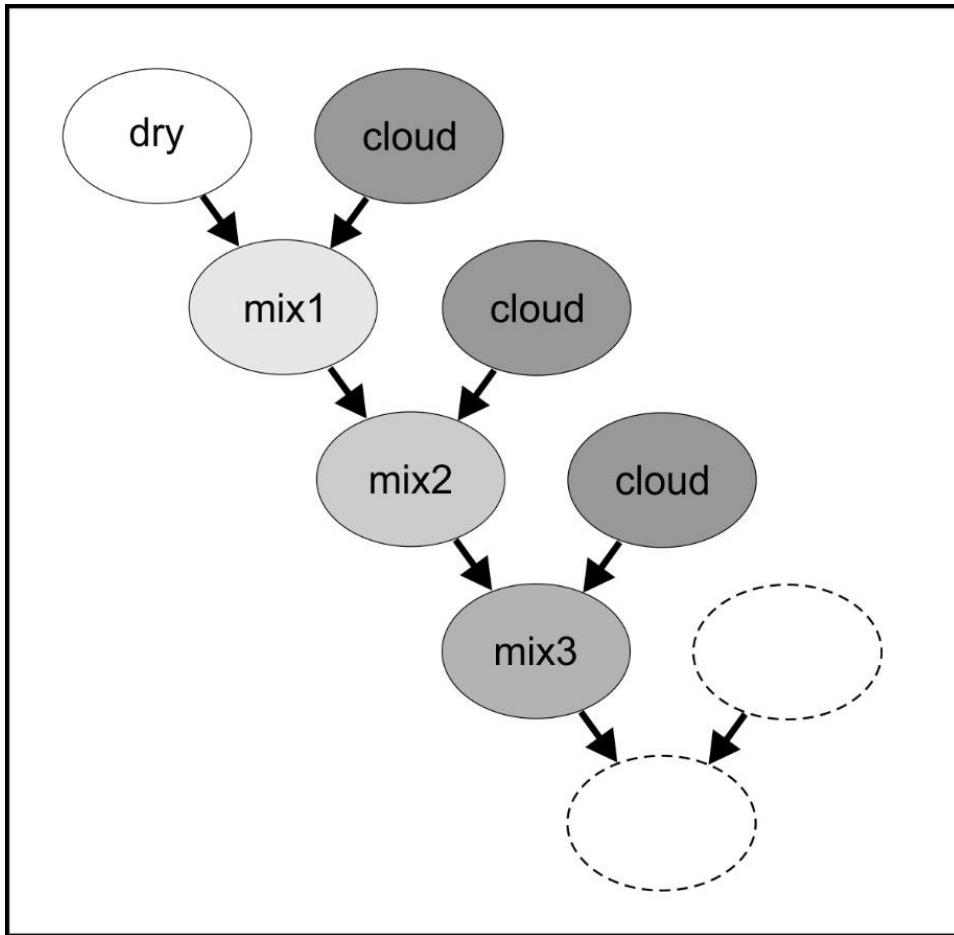
1
2

3 **Figure 6.** Simulation of (a) droplet number concentration and (b) liquid water mixing ratio, (c) integral droplet
4 diameter, (d) extinction coefficient, (e) mean volume diameter, (f) time of phase relaxation, (g) relative humidity in
5 the mixed volume before droplet evaporation RH_{m0} and at the equilibrium state RH_m , (h) final temperature T_m versus
6 ratio of mixing μ formed after homogeneous and extreme inhomogeneous mixing between dry and cloudy parcel with
7 monodisperse droplets. The calculations were performed for $RH_2=0.9$; $D_1=10\mu\text{m}$, $N_1=500\text{cm}^{-3}$; $T_1 = 0\text{C}$; $T_2 = -10\text{C}$,
8 -5C , 0C ; $H=1000\text{m}$.



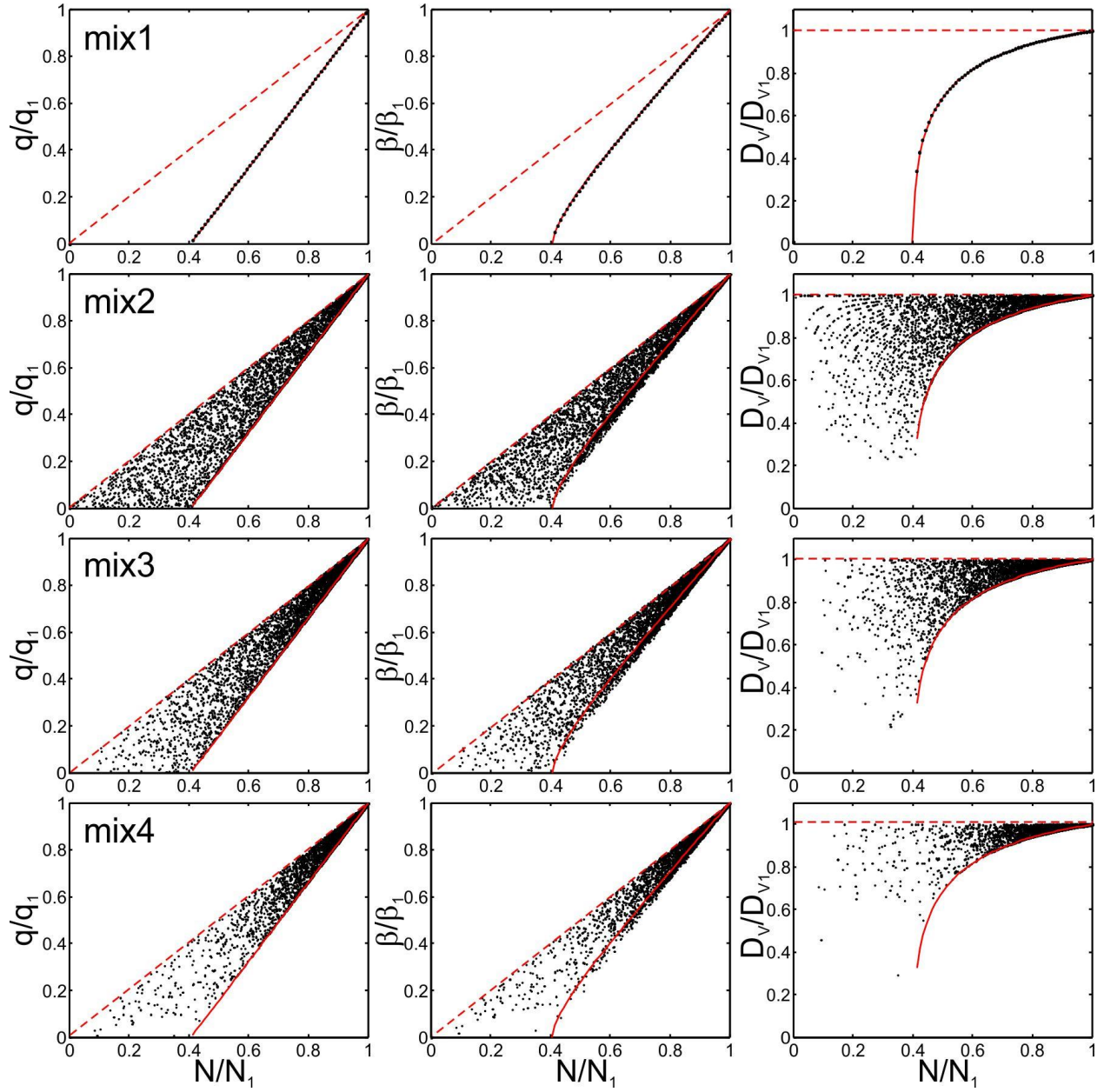
1
2

3 **Figure 7.** Effect of temperature difference between cloud and entrained air on mixing. The calculations were performed
 4 for initial temperatures T_2 : (1) -10C ; (2) -5C ; (3) 0C . Grey circles indicate extremely inhomogeneous mixing on line 1
 5 at the AB interval. The rest cases on extremely inhomogeneous mixing are indicated by open circles. The initial
 6 conditions used for the calculations were: $H=1000\text{m}$, $RH_2=90\%$; $D_1 = 10\mu\text{m}$, $N_1 = 500\text{cm}^{-3}$, $T_1=0\text{C}$.



1
2
3
4
5

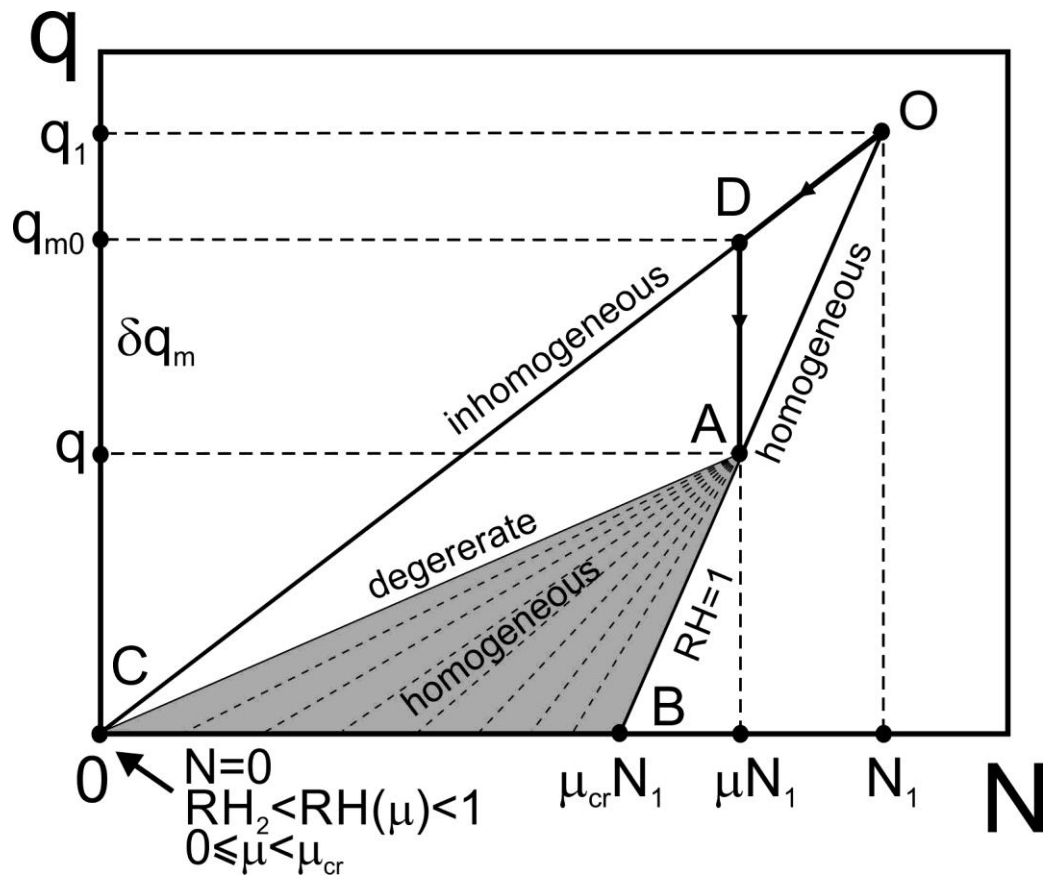
Figure 8. Conceptual diagram of cascade mixing of the out-of-cloud entrained parcel with the cloudy environment



6

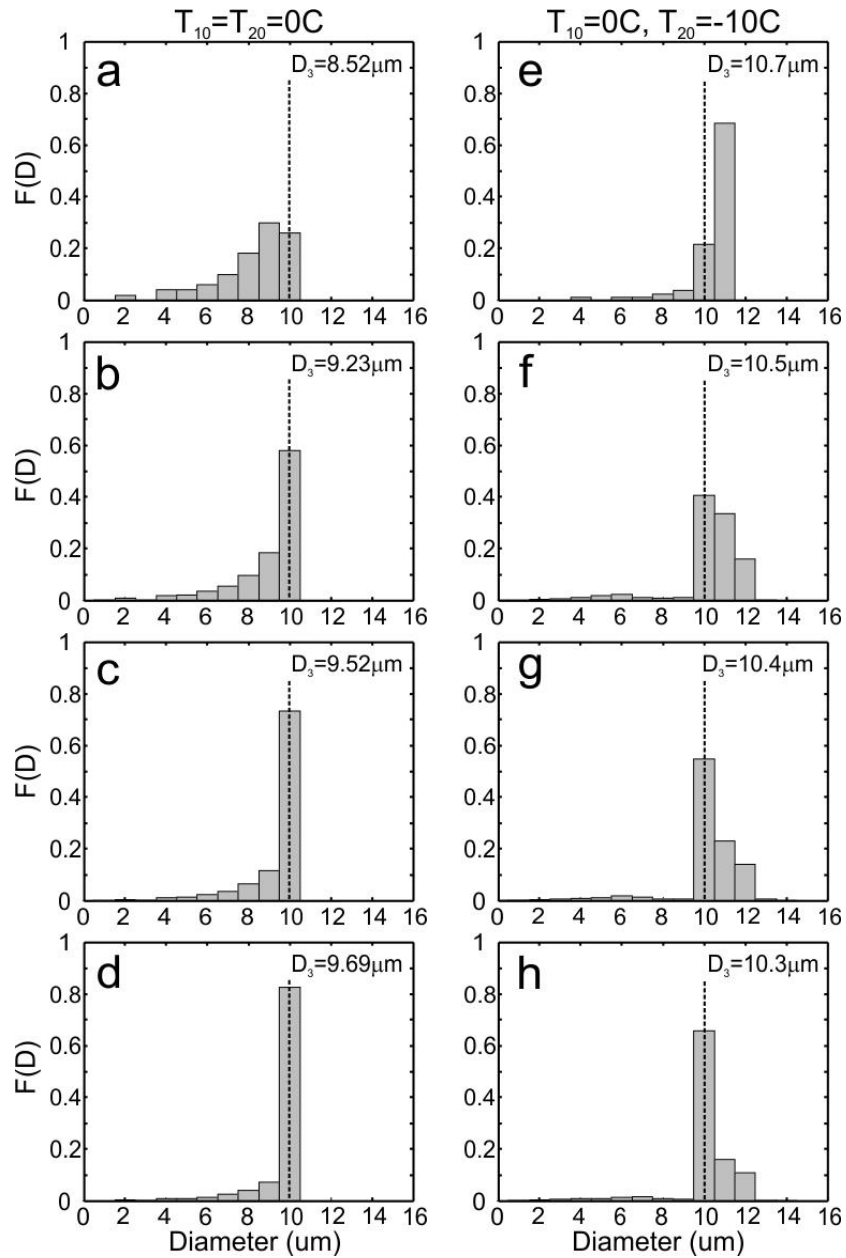
7 **Figure 9.** Simulation of stochastic mixing corresponding to stages 1-4 as indicated in Fig.8. Solid red lines indicate
 8 the normalized dependences q , β , D_v vs. N for the primary stage of homogeneous mixing. Dashed red lines indicate
 9 the same dependences for inhomogeneous mixing. The initial conditions used for the simulations were: $H=1000\text{m}$,
 10 $T_1 = T_2 = 0\text{C}$; $RH_2=0.5$; $D_1 = 10\mu\text{m}$, $N_1 = 500\text{cm}^{-3}$.

11



1
2
3
4
5

Figure 10. Conceptual diagram explaining breaking the functional relationships between the microphysical moment during progressive missing (see text).



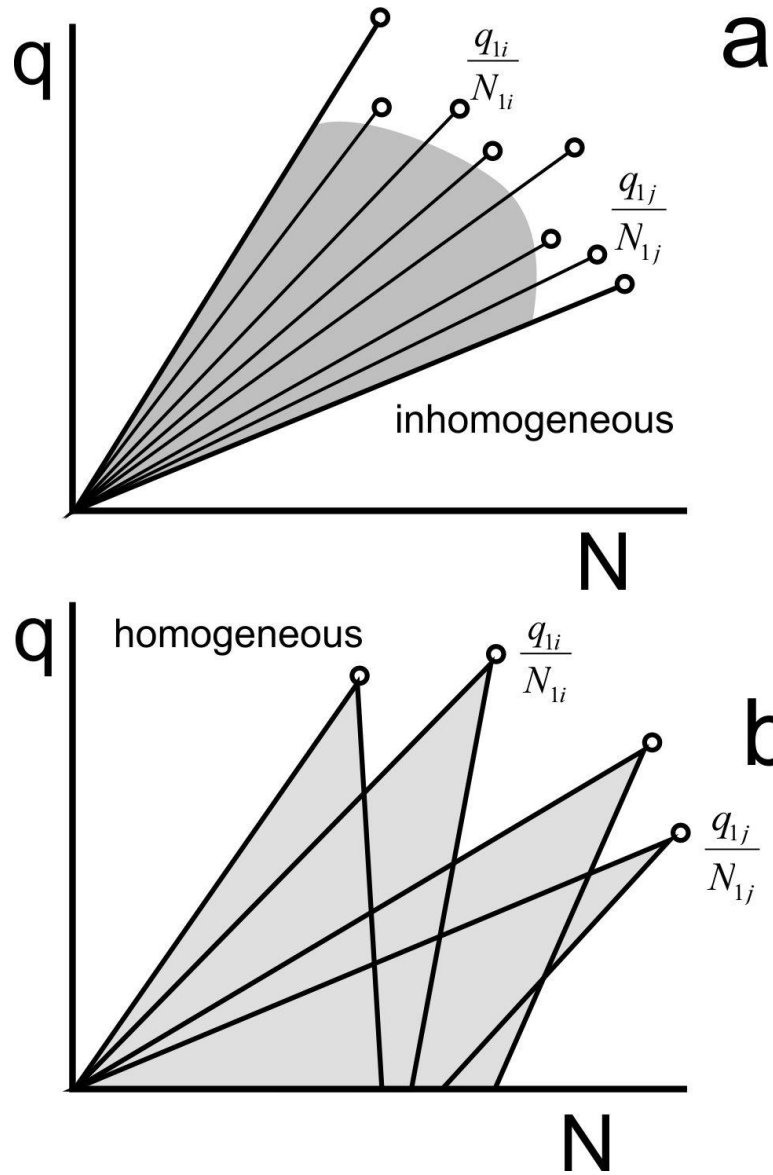
2

3

4 **Figure 11.** Droplet size distributions formed during the progressive homogeneous mixing corresponding to the (a,e)5 primary stage; (b,f) 2nd stage; (c,g) 3rd stage; (d,h) 4th stage. Left column (a,b,c,d) corresponds to the case, when the6 cloud temperature is equal to the dry air temperature $T_1 = T_2 = 0^\circ\text{C}$.; right column (e,f,g,h) corresponds to the case7 when $T_1 = 0^\circ\text{C}$, $T_2 = -10^\circ\text{C}$. For both cases the simulation was performed for $D_1 = 10\mu\text{m}$; $N=500\text{cm}^{-3}$; $RH_2=0.9$.

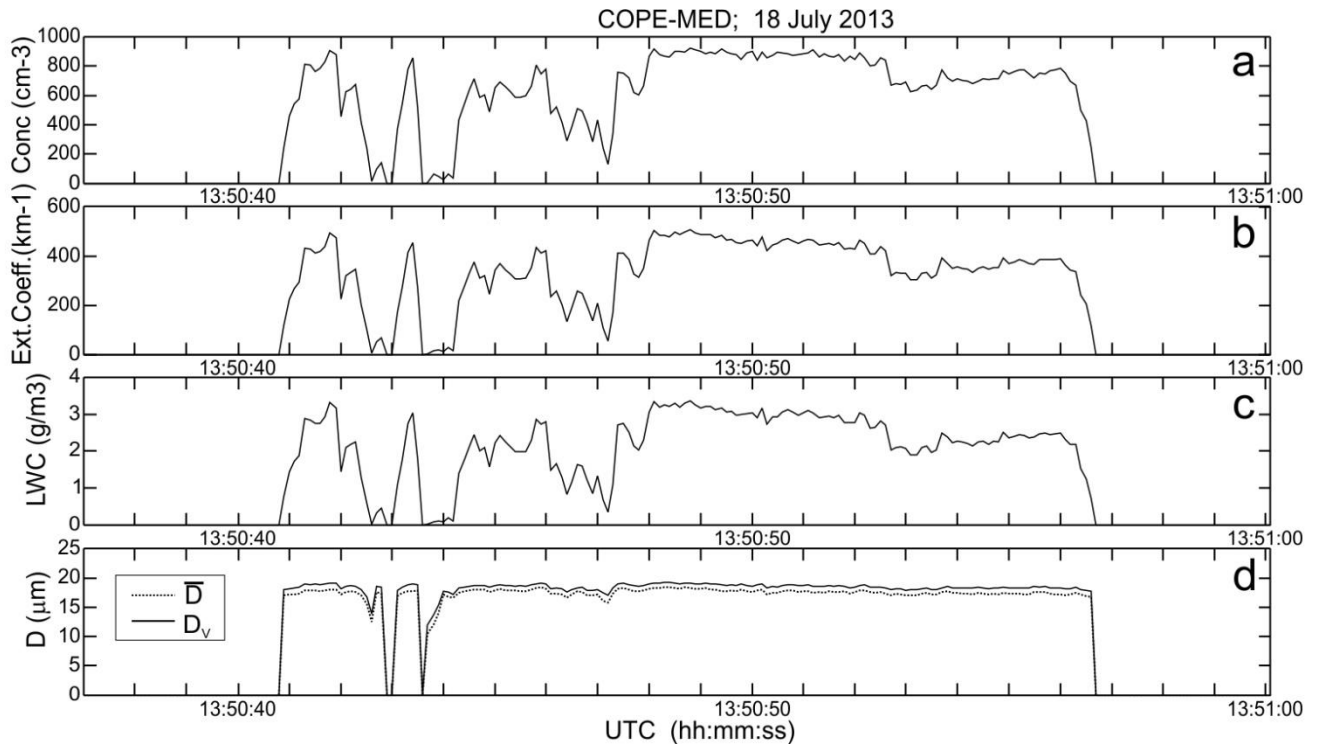
8

1
2



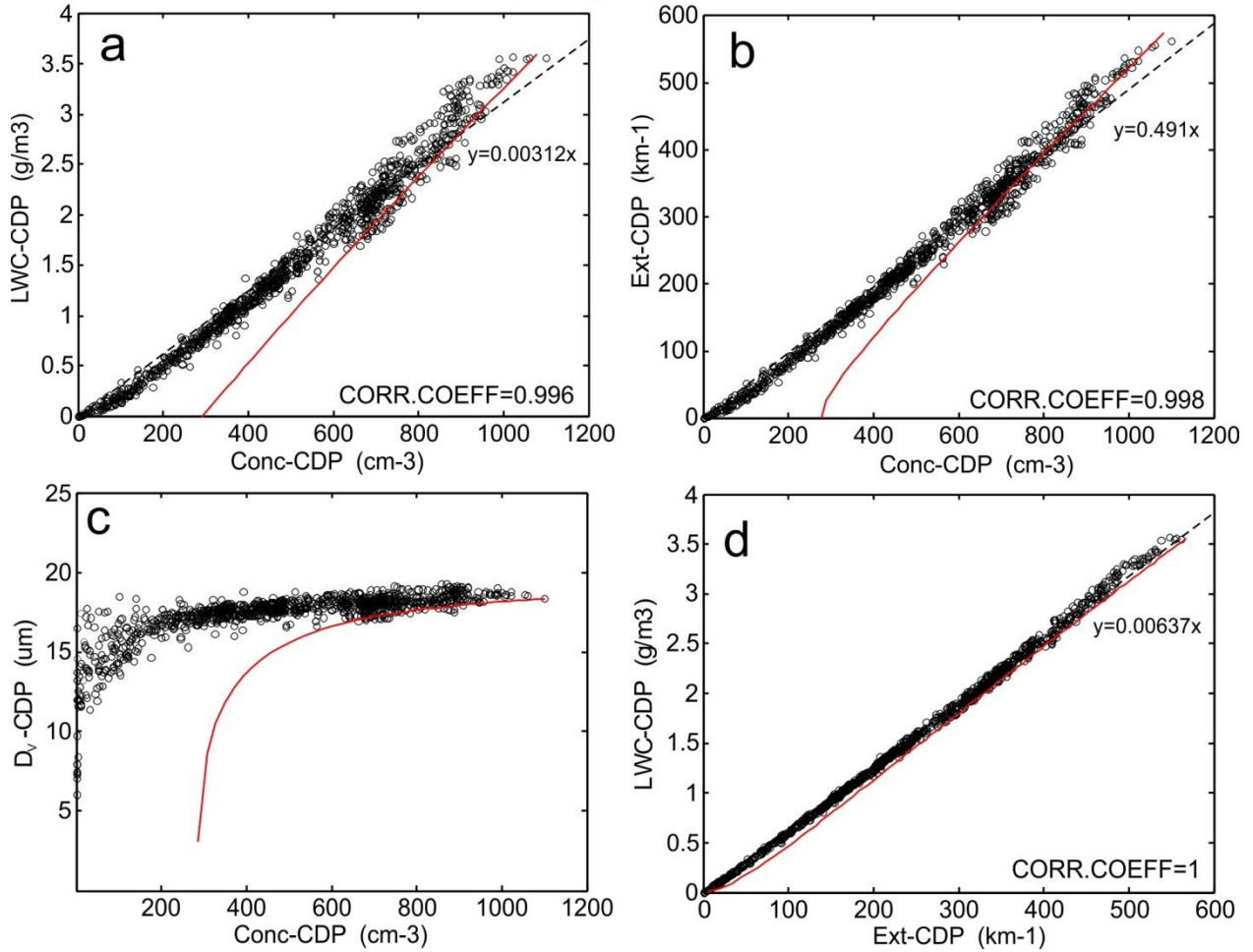
3
4
5
6
7
8

Figure 12. Conceptual diagrams of scattering of measurements of q versus N for (a) extreme inhomogeneous and (b) homogeneous mixing.



1
 2 **Figure 13.** Spatial changes of particle concentration (a), extinction coefficient (b), liquid water content (c) and average
 3 and mean mass diameter (d) during transit through one of the convective clouds measured by CDP. The measurements
 4 were conducted during the COPE-MED project on 18 July, 2015. The sampling rate 10Hz (~10m spatial resolution).
 5 $H=5500\text{m}$, $T=-12\text{C}$, $RH=0.2$.

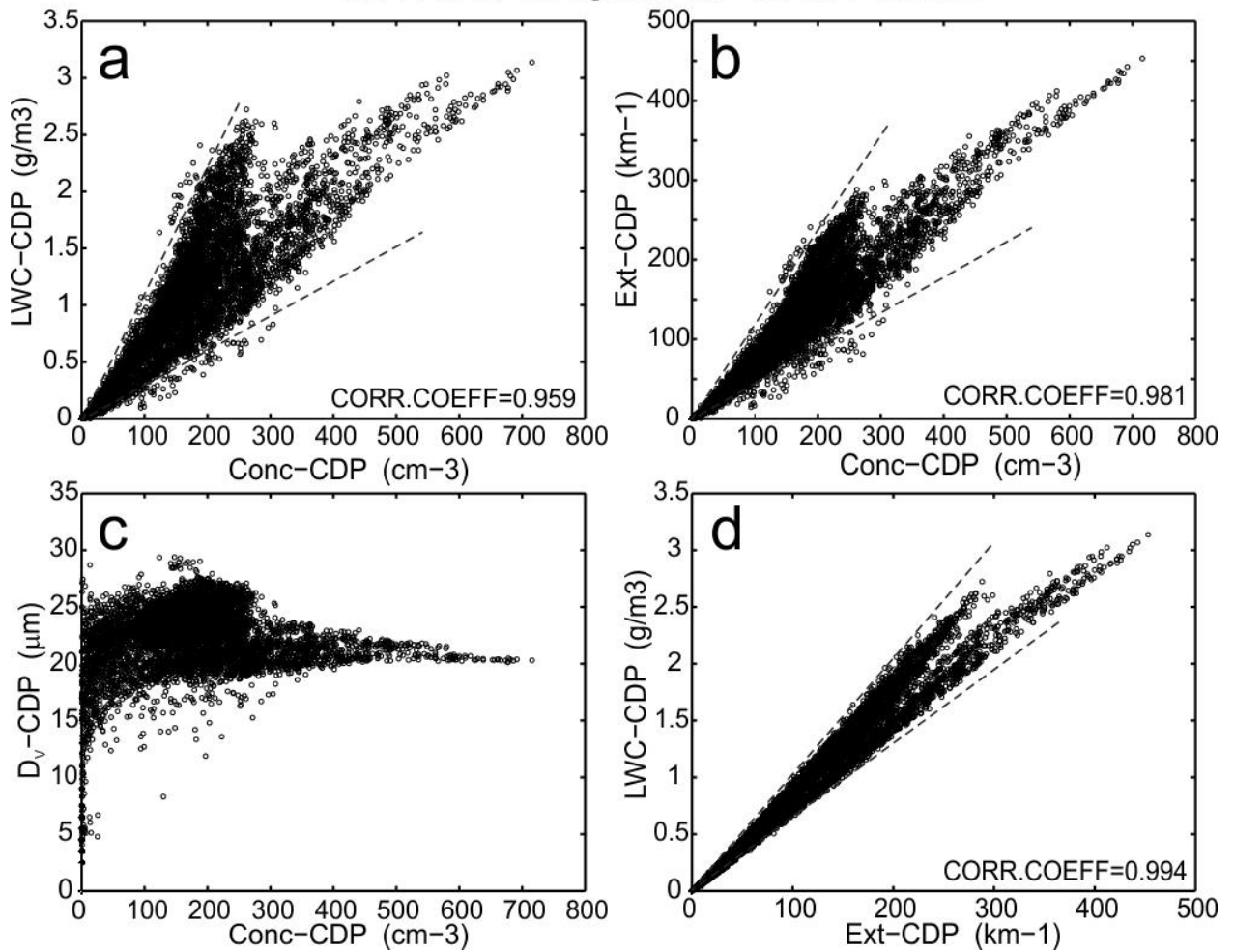
6



1
2
3
4
5
6
7
8
9

Figure 14. Relationships between (a) $LWC(N)$; (b) $\beta(N)$; (c) $D_v(N)$; (d) $LWC(\beta)$ calculated from the CDP measurements obtained during sampling several convective clouds. The measurements were conducted during the COPE-MED project on 18 July, 2015, $H=5500m$, $T=-12C$, $RH=0.2$. The measurements were sampled at 10Hz (~10m spatial resolution). Dashed lines are linear regressions. Red lines indicate primary inhomogeneous mixing dependencies calculated for the same environmental conditions.

COPE-MED; 02 August 2013; 13:25:01-15:38:06



1
2
3
4
5
6
7
8
9
10

Figure 15. Relationships between (a) $LWC(N)$; (b) $\beta(N)$; (c) $D_v(N)$; (d) $LWC(\beta)$ calculated from the CDP measurements sampled during traverse through 45 convective clouds. The measurements were conducted during the COPE-MED project on 02 August, 2015. Dashed lines indicate (a), (b) and (d) indicate the sectors, where the majority of the points are scattered. The altitude of sampling varied in the range $3000\text{m} < H < 4500\text{m}$, temperature $-11\text{C} < T < 0\text{C}$, relative humidity in the vicinity of clouds $15\% < RH < 65\%$. The measurements were sampled at 10Hz (~10m spatial resolution).

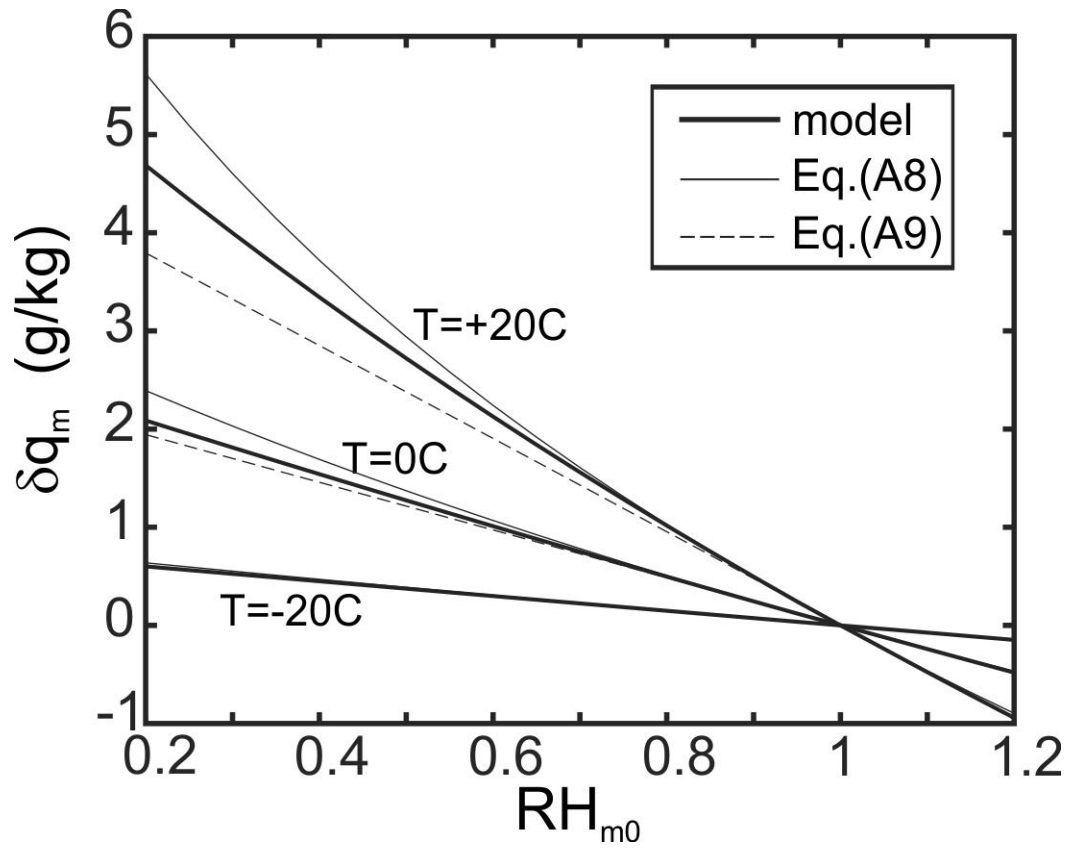


Figure A1. Amount of evaporated liquid water δq_m required for saturation of a cloud volume with initial humidity RH_m . Comparisons of the modeled δq_m and that calculated from Eqs. (A8) and (A9) for three temperatures $T_{m0} = -20\text{C}$, 0C and 20C . Calculations were performed for $P=880\text{mb}$.